https://doi.org/10.5194/egusphere-2026-1018
Preprint. Discussion started: 6 March 2026

Alluvial river-channel width: transient adjustment and dynamic equilibrium

Andrew D. Wickert[1,2,3], Jabari C. Jones[1,2,4], Devon Libby[5], Phillip H. Larson[5], Katherine R. Barnhart[6,7,a], Maximillian S. Van Wyk de Vries[1,2,8,9], and Taylor F. Schildgen[3,10]

[1]Saint Anthony Falls Laboratory, University of Minnesota, Minneapolis, MN 55414, USA
[2]Department of Earth and Environmental Sciences, University of Minnesota, Minneapolis, MN 55455, USA
[3]Sektion 4.6: Geomorphologie, GFZ Helmholtz-Zentrum für Geoforschung, Potsdam, 14473, Germany
[4]Department of Earth and Oceanographic Science, Bowdoin College, Brunswick, ME 04011, USA
[5]EARTH Systems Laboratory, Minnesota State University, Mankato, MN 56001, USA
[6]Cooperative Institute for Research in Environmental Sciences, University of Colorado, Boulder, CO 80309, USA
[7]Department of Geological Sciences, University of Colorado, Boulder, CO 80309, USA
[8]Department of Geography, University of Cambridge, Cambridge, CB2 3EL, UK
[9]Department of Earth Sciences, University of Cambridge, Cambridge, CB3 0EZ, UK
[10]Institut für Geowissenschaften, Universität Potsdam, Karl-Liebknecht-Str. 24-25, 14476 Potsdam, Germany
[a]now at: U.S. Geological Survey, Geologic Hazards Science Center, Golden, CO 80401, USA

Correspondence: Andrew D. Wickert (awickert@umn.edu)

Abstract. Alluvial river channels naturally widen and narrow as large floods scour banks and smaller ones supply sediments that help build bars and channel margins. Despite substantial advances into the controls on the equilibrium width of river channels, relatively little theory underpins our knowledge on transient river-channel-width evolution. Such a knowledge gap inhibits us from predicting the impacts of present-day nonstationary hydrology on river-channel stability and geomorphic change. Here we present a unified approach to model transient channel widening, via erosion of cohesive banks and mobilization of noncohesive clasts, and narrowing, via lateral diffusion of sediment that attaches to the banks. The resultant model can take a full hydrograph as input, allowing the hydraulic geometry and associated "geomorphically effective" water discharge to emerge dynamically. Stable widths develop via the inverse relationship between channel width and flow depth, and therefore, shear stress on the channel margins. Equilibrium solutions closely approximate data and theory on channels with both gravel and mud banks, and we compare transient solutions to the rapidly widening Minnesota and Cannon Rivers (Minnesota, USA) and the narrowing Green River and Diamond Fork (Utah, USA). Documented Python source code to run these computations is available from GitHub and Zenodo via the "OTTAR" package, and may be installed via pip from PyPI.

1 Introduction

Alluvial rivers flow through self-formed open channels that transmit water and sediment as they sculpt the landscape. "Self-formed" means that river channels adjust their slopes, hydraulic geometries (widths and depths, for an idealized rectangular channel), and boundary roughness, such that they are able to transmit the supplied sediment with the supplied water (Mackin, 1948; Lane, 1955; Pizzuto, 1992). All of these variables affect the conveyance capacity of a river – the water discharge that it

https://doi.org/10.5194/egusphere-2026-1018
Preprint. Discussion started: 6 March 2026

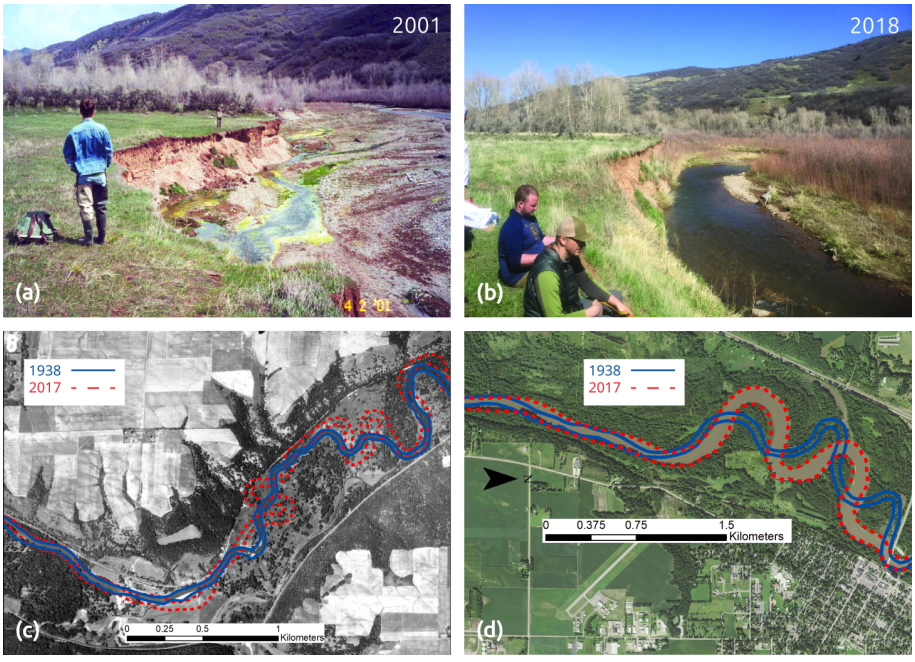

Figure 1. Examples of channel narrowing and widening. **(a)** Diamond Fork River, Utah in April, 2001, showing a braidplain that occupies the entire valley bottom; photo taken by Robert Gecy, U.S. Forest Service. **(b)** Diamond Fork River in April, 2018, after the braidplain became vegetated and the channel reduced to a single thread; photo taken by Jabari Jones. **(c)** Channel margins of the Cannon River, Minnesota, downstream from Welch, MN, in 1938 and 2017. Note channel widening and meander migration; the background is a 1938 aerial photograph. **(d)** Channel margins of the Minnesota River near Le Sueur, MN, in 1937 and 2013 showing channel widening; the background is 2013 aerial photograph (Libby, 2018).

is able to carry before flows exit the channel and go overbank. Furthermore, they impact the distribution of shear stresses on the channel walls, which produces a two-way coupling between river flow and the evolution of channel form (Popović et al., 2021).

Alluvial rivers can adjust their hydraulic geometries over shorter time scales such as those associated with individual flood events (Wolman and Gerson, 1978; Andrews, 1982; Pizzuto, 1994; Ruiz-Villanueva et al., 2018; Phillips et al., 2024) or over decades (Wolman and Gerson, 1978; Pizzuto, 1994; Slater and Singer, 2013; Schottler et al., 2014; Slater et al., 2015; Lauer et al., 2017; Donovan et al., 2019; Slater et al., 2019). This dynamic behavior contrasts to the thousands of years commonly required to regrade their slopes – and therefore, long profiles (e.g., Naito and Parker, 2019, 2020). This difference can arise because changes in hydraulic geometry affect only the local reach rather than requiring a long-term balance with full river-scale sediment supply and dynamics, as is the case for long-profile adjustment (e.g., Mackin, 1948; Wickert and Schildgen, 2019).

Channel width should also adjust more dynamically than channel depth (Pizzuto, 1992). Widening or narrowing a channel requires erosion or deposition across the channel banks, which are short relative to the widths of the floodplain (Knox, 1972; Pizzuto, 1986, 1992) and channel. Therefore, modifying width requires less erosion or deposition than modifying channel

https://doi.org/10.5194/egusphere-2026-1018
Preprint. Discussion started: 6 March 2026

depth. Additionally, changes in river-bed and floodplain elevations affect river slope, whose continuity imposes a stabilizing feedback: changes in channel depth must eventually engage with the slower process of regrading the long profile. Even with these physical constraints, changes to the elevation of the channel and/or floodplain may be rapid, as is observed following large anthropogenic changes to sediment supply (Gilbert, 1917; James, 1991; Wood, 2023). Nonetheless, improving our ability to forecast changes to river-channel width should address the commonly most dynamic degree of freedom that rivers possess over time scales relevant to human infrastructure as well as to modern environmental and climatic change.

The speed with which hydraulic geometry changes has significant practical and geological consequences. Based on data compilations from the conterminous USA, Slater et al. (2019) showed that river-channel cross sections expand and contract in response to annual-to-decadal oscillations in climate that drive precipitation. Such changes add an oft-overlooked channel-morphological factor that affects flood probability (Slater et al., 2015; Ahrendt et al., 2022). Furthermore, channel-width adjustments are accommodated by bank and/or bluff erosion (Kelly and Belmont, 2018), which may affect water quality (Belmont et al., 2011b; Daly et al., 2015b) and habitat for endemic species (Hornbach et al., 2018). Channel widening can have more direct impacts on ecosystems as well, through the loss of riparian vegetation and increased solar incidence on the stream channel (Belsky et al., 1999; Justice et al., 2017). Over longer time scales, width adjustments affect the basal shear stress and sediment-transport capacity of a river (Parker, 1978a; Wickert and Schildgen, 2019), and non-steady-state river widths could activate nonlinear responses that amplify or dampen rates of river long-profile evolution in response to external perturbations (Pfeiffer et al., 2017).

Despite the dynamism of channel width and its importance in both hydrology and geomorphology, we currently have no general, tested theory to explain transient channel-width evolution. Here we design and build a flux-based theory that combines widening via bank-material entrainment and narrowing due to net sediment diffusion towards the river banks. Both our new dynamic theory and the existing static threshold-stress theory (Parker, 1978a; Dunne and Jerolmack, 2018) are 0-dimensional theories: they balance scalars without requiring explicit discretization of the river channel. Therefore, they allow us to focus on the general dynamics governing river width. We demonstrate that equilibrium solutions to our dynamic-width theory lie close to those based on static threshold-stress theory (Parker, 1978a; Dunne and Jerolmack, 2018), and we calibrate the model parameters to data from four distinct river reaches (Table 2).

1.1 Equilibrium width

Prior to the present work on transient river-channel-width changes, geomorphologists built semi-empirical relationships, mechanistic theory, and physical experiments to understand river-channel width and its equilibrium state (e.g., Lacey, 1930; Métivier et al., 2017). Although much of this work has focused exclusively on the equilibrium state (e.g., Parker, 1978a; Phillips et al., 2022), some studies include the dynamics to approach this equilibrium (Pizzuto, 1990; Naito and Parker, 2019, 2020; Popović et al., 2021). In general, our current understanding of equilibrium river-channel hydraulic geometry enables us to link basic field observables to bankfull and geomorphically effective discharge (Leopold and Maddock, 1953; Wolman and Miller, 1960) and to partition shear stress and stream power across the channel boundaries (Parker, 1978a; Whipple and Tucker, 1999).

https://doi.org/10.5194/egusphere-2026-1018
Preprint. Discussion started: 6 March 2026

Seven decades ago, Leopold and Maddock (1953) demonstrated that channel width, b, increases downstream (i.e., with increasing bankfull discharge, Q) as $b \propto Q^{0.5}$. This square-root scaling matched experimental and mechanistic research into the equilibrium self-formed hydraulic geometry of river channels in silt (Lacey, 1930). Such findings quantify the scaling relationship behind an everyday observation in geomorphology: rivers that carry more water are typically wider.

Following this work, researchers began to produce theory on alluvial-river equilibrium width (Glover and Florey, 1951; Parker, 1978a; Eaton et al., 2004; Seizilles et al., 2013; Phillips and Jerolmack, 2016; Métivier et al., 2017; Pfeiffer et al., 2017; Dunne and Jerolmack, 2018, 2020; Phillips et al., 2022). They suggested that rivers' widths adjust such that, at bankfull flow conditions, shear stresses on their banks equal equal the stress required to initiate detachment of bank material. This can relate to a Shields criterion for noncohesive material (Parker, 1978a) or a dimensional critical shear stress for muddy banks (Dunne and Jerolmack, 2018).

Pizzuto (1990); Parker et al. (2011), (Eke et al., 2014a), and Naito and Parker (2019, 2020); and Popović et al. (2021) followed on this research with mechanistic theory, numerical modeling, and experimental evidence for the transient and equilibrium behavior of river channels. Pizzuto (1990) distributed shear stress across the wetted perimeter of a channel with a noncohesive gravel bed and banks, and enabled lateral erosion through bank slumping based on a Mohr–Coulomb criterion. These channels approached an equilibrium form reminiscent of, though not exactly equaling, the Parker (1978a) theory. Naito and Parker (2019, 2020) simulated the specific case of a meandering river, developing an equilibrium width through the combined processes of cut-bank erosion and point-bar deposition, building upon foundational work by Parker et al. (2011) and Eke et al. (2014a). Popović et al. (2021) performed a series of laminar-flow experiments that included both channel widening, through entrainment of bank materials, and narrowing, through lateral diffusion of sediment. Although they were performed in straight laboratory channels with thin and slow laminar flows relative to turbulent field conditions, these experiments demonstrated the flux balance required to produce channel morphological equilibria that evolved to maintain boundary shear stresses near the threshold for sediment motion (Parker, 1978a).

Over the past ∼2 decades, geomorphologists expanded both empircal and theoretical approaches to rivers with cohesive beds and banks – that is, those for which erosive widening rate is limited by the rate detachment of cohesive materials. In the context of alluvial rivers, this theory relates to erosion of cohesive muddy streambanks; to date, however, the literature has focused primarily on bedrock rivers. Wobus et al. (2006) and Turowski (2009) developed stream-power and shear-stress (respectively) approaches to erosion across the full wetted perimeter of a bedrock river—a full transient theory—and demonstrated how hydraulic geometry would respond to increasing tectonic uplift rates by causing the channel to narrow and deepen. Turowski et al. (2007), Yanites and Tucker (2010), and Yanites (2018) developed physically reasonable optimization approaches to river-channel width and demonstrated that they likewise reproduce major features of observed bedrock-river hydraulic geometry.

At a finer scale, local streambank-erosion forecasts—typically requiring mapping and in-situ tests of streambank properties—can aid understanding of equilibrium river-channel geometry by building projections of bank failures (e.g., Simon et al., 2000; Duan, 2005; Daly et al., 2015b; Klavon et al., 2017). Process-based models can capture the meandering process as a fundamental channel-width feedback in a river with asymmetrical flow (Parker et al., 2011). These latter models have been built around parameterizations of slump blocks and their ability to armor eroding banks (Eke et al., 2014a, b), and they have been

https://doi.org/10.5194/egusphere-2026-1018
Preprint. Discussion started: 6 March 2026

employed to demonstrate how width–erosion–deposition feedbacks generate bankfull hydraulic geometry (Naito and Parker, 2019, 2020) and river-channel lateral mobility (Eke et al., 2014a). These latter approaches generate low-gradient meandering rivers with dynamically self-formed widths that can support transient evolution, alongside the co-development of the channel long profile and floodplain.

1.2 Transient channel adjustment as a possible cause for departure from equilibrium theory

The aforementioned equilibrium-width theory posits that rivers adjust towards a deterministic hydraulic geometry over time. However, by replacing an idealized steady water-discharge forcing with a realistic hydrograph, complete with variable flood magnitudes and periods of low flow, one may intuit that real rivers exist in something more akin to a quasi-equilibrium state governed both by the flow history and the rate of river-channel adjustment to these flows (Figure 2). Alluvial river channels widen—sometimes dramatically (Schumm and Lichty, 1963)—during large floods (Pizzuto, 1994; Montgomery and Gran, 2001; Pitlick et al., 2013). During more modest flood events, they can narrow as sediment is transported to and deposited against the banks (Andrews, 1982; Pizzuto, 1994; Jones et al., 2023) (Figure 3). Vegetation, whose stems in turn can slow flow and further confine the channel (Wolman and Gerson, 1978; Gran and Paola, 2001; Tal and Paola, 2007), can also trap and stabilize this sediment, enhancing river-channel narrowing (Allmendinger et al., 2005; Tal and Paola, 2010; Gurnell, 2014).

Although channel widths do evolve in two-dimensional (depth-averaged map-view) simulations (Laz, 2012; Nicholas, 2013), we currently lack a physically based cross-sectional model that resolves transient river-width dynamics. This is a major gap in our understanding of channel hydraulic geometry and its evolution. Parameterizations of bank stresses and channel–floodplain feedbacks in map-view models (e.g., Lesser et al., 2004; Deltares, 2025) can demonstrate emergent channel-width dynamics (Nicholas, 2025). However, building a detailed cross-sectional model forces us to consider the explicit mass balances and feedbacks that drive transient river widening and narrowing. Such a model could improve our understanding of hydrologic-geomorphic coupling, its modulation by river-control structures and changing climate, and its impact on ecosystems and flood hazards (Phillips et al., 2024).

We hypothesize that transient river-width response to a time-variable (i.e., realistic) hydrograph contributes to the observed order-of-magnitude scatter in observed river widths and associated water-induced shear stresses around an equilibrium value (Phillips and Jerolmack, 2016; Métivier et al., 2017, Figs. 4b and 2, respectively). This hypothesis implies that river widths exist in a state of quasi-equilibrium with respect to any dominant "channel-forming" flow (sensu Wolman and Miller, 1960) (see also: Andrews, 1980; Hassan et al., 2014). Consequently, a theory for how river-channel width evolves transiently may not only improve predictions of flooding, but also improve linkages between field observations and theory describing equilibrium hydraulic geometry.

1.3 Transient-width theory

We developed a theory for coupled river-channel widening and narrowing in alluvial rivers, motivated by four goals: (1) generating accurate river-morphology forecasts for informed environmental management, (2) understanding how flow variability and lagged geomorphic response may perturb observed river-channel widths away from predictions from equilibrium theory, (3)

https://doi.org/10.5194/egusphere-2026-1018
Preprint. Discussion started: 6 March 2026

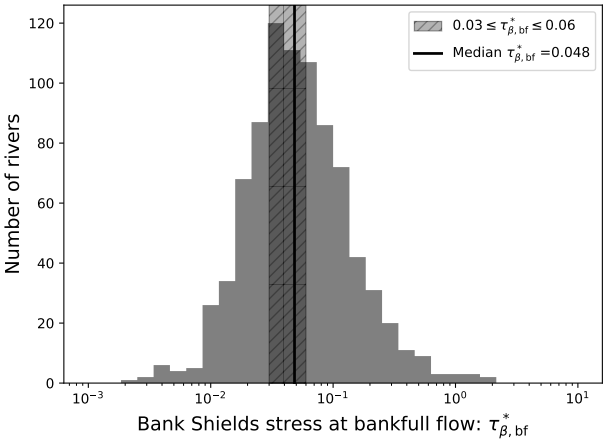

Figure 2. Gravel-bed rivers have bankfull basal Shields stresses that are approximately log-normally distributed. Observations (Figure 2) indicate that median bed Shields stress corresponds to the median stress at which gravel begins to be mobilized on the channel walls, in agreement with theory (Parker, 1978a). Initiation of motion occurs at a Shields stress τ^*_β in the range of 0.03 (Parker, 1990) to 0.06 (Shields, 1936), with β indicating that this is the stress exerted on the channel banks. Here we propose that at least some of the 2 orders of magnitude spanned by these data could be explained by transient responses to recent streamflow changes, such as a wider channel due to a recent major flood or a narrower channel caused by significant bank deposition during moderate-intensity flow events (Figure 3). Similar scatter about a mean likely exists for sand-bed rivers, but only few measurements on threshold entrainment stress for muddy bank materials exist, meaning that we cannot separate questions of hysteresis from those of critical shear stress (Dunne and Jerolmack, 2020), and as a result, we do not analyze sand-bed systems. Data from Phillips et al. (2022).

better understanding internal feedbacks in river morphodynamics, and (4) providing a generalizable modeling approach while limiting input-data requirements. The widening rate is set by the slower of two processes: entrainment of noncohesive clasts on the bank and erosion of cohesive bank material. Narrowing is accomplished by lateral diffusion of sediment towards the banks (Popović et al., 2021), modulated by grain cohesion and vegetation trapping. These widening and narrowing processes interact by altering flow depths and therefore wall stresses; and under steady flow conditions, these feedbacks can eventually produce predicted (e.g., Parker, 1978a; Dunne and Jerolmack, 2018) steady-state alluvial channel widths.

Here we focus exclusively on river-channel lateral dynamics. River channels may narrow with rapid incision (Rinaldi, 2003; Pfeiffer et al., 2017), creating high banks that inhibit widening (Bufe et al., 2016; Malatesta et al., 2017). Conversely, during times of rapid aggradation, river channels may widen into broad, braided forms (Germanoski and Schumm, 1993). These observations highlight the feedbacks between lateral and vertical fluxes of sediment in setting alluvial-river hydraulic geometry. Nonetheless, we hold bed elevation constant in our analyses and discussion here to focus on and isolate the question of transient channel width.

https://doi.org/10.5194/egusphere-2026-1018
Preprint. Discussion started: 6 March 2026

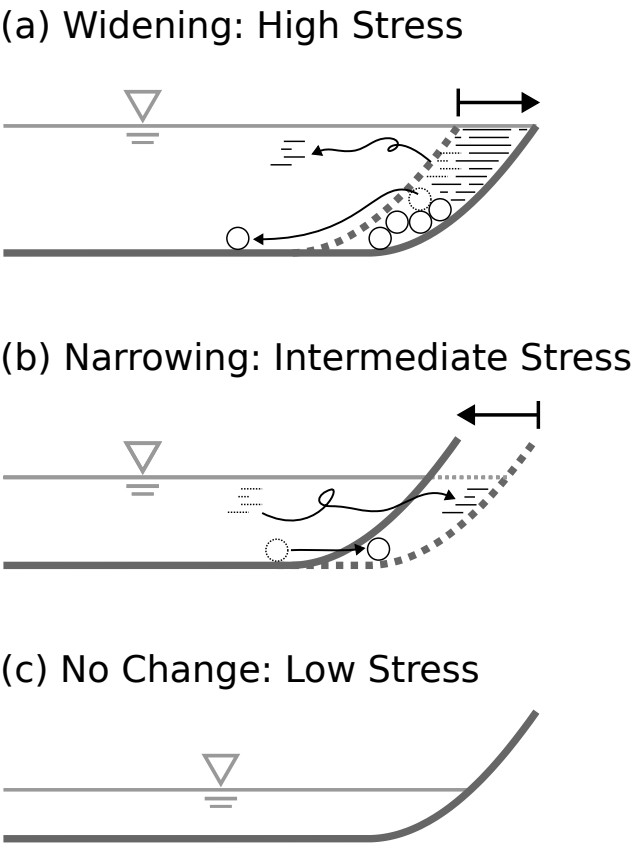

Figure 3. Conceptual model for modes of river-channel widening and narrowing and their connections with flow stage. **(a)** High flows produce stresses that exceed erosional thresholds and lead to net river-channel widening. **(b)** Intermediate flows can mobilize sediment that diffuses towards the banks, causing channel narrowing, but do not apply enough stress to the banks to cause much erosion. Here we depict deposition along the whole height of the bank despite the lower water level to be consistent with our use of channel width as a single parameter in the formulation (see Section 3.2). These depositional processes may also occur during channel widening (a), but in this case occur more slowly than lateral erosion. **(c)** The lowest flows are unable to significantly change channel morphology. Realistically, these flows can permit vegetation growth on banks and bars, thereby stabilizing the channel; however, to maintain a more straightforward model, here we simulate this process without explicit consideration of vegetation dynamics (see Section 5).

2 Approach

As a framework to model river-channel width and its variability, we define channel width at time t_i, $b_i = b(t_i)$, as the sum of a given initial width, $b_0 = b(t_0)$, and the time integral of the rate of width change, $\dot{b}$, from t_0 to t_i:

$$b_i = b_0 + \int_{t_0}^{t_i} \dot{b}\,\mathrm{d}t. \tag{1}$$

https://doi.org/10.5194/egusphere-2026-1018
Preprint. Discussion started: 6 March 2026

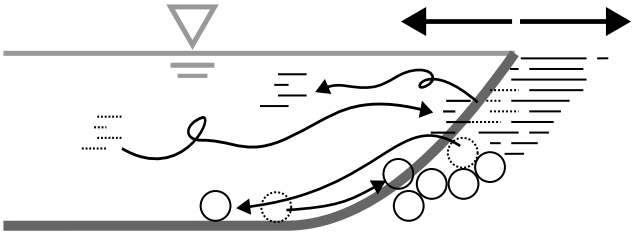

Figure 4. Equilibrium river width is maintained by a balance between drivers of widening and narrowing. Here, an equal amount of material is leaving and re-entering the banks via both suspended load (cohesive) and bed load (noncohesive) mechanisms. Because the relative strength of drivers of erosion (widening) and deposition (narrowing) varies with streamflow, which varies in rivers even when it is statistically stationary, such an equilibrium in real rivers should be dynamic: Under statistically constant hydrological forcing, channel width should vary about a mean value, but depend on recent flow and sediment-transport events.

From this starting point, we further decompose the rate of overall width change into widening ($\dot{b}_w$) and narrowing ($\dot{b}_n$) terms.

$$\dot{b} = \dot{b}_w + \dot{b}_n. \tag{2}$$

We use a widening-positive sign convention such that $\dot{b}_w$ must always be ≥ 0 and $\dot{b}_n$ must always be ≤ 0.

Having formulated Equation 2, we next ask whether its solutions are stable or unstable. As noted above, current data-supported theory demonstrates that alluvial river channels commonly maintain their widths near threshold-of-motion conditions for bank materials during bankfull flows (Parker, 1978a; Phillips and Jerolmack, 2016; Dunne and Jerolmack, 2018; Dunne et al., 2022; Phillips et al., 2022). Furthermore, strong trends exist between water discharge and channel hydraulic geometry (Leopold and Maddock, 1953), which likewise relate to conditions required for bank-material entrainment (Lacey, 1930; Glover and Florey, 1951; Métivier et al., 2017). Additional support for persistent river-channel widths exist from global remotely sensed data (Lin et al., 2020) and observations of preserved cut-off river meanders from the geological past (e.g., Knox, 1985, 2000). We find that both evidence and theory support that a stable solution exists in which $\dot{b} \to 0$, and therefore, widening and narrowing come into a balance. Such a stable solution likewise follows from past transient modeling investigations into meandering rivers (Parker et al., 2011; Eke et al., 2014a, b; Naito and Parker, 2019, 2020).

The obvious solution to the above thought exercise belies the two features of existing equilibrium-width theory that it illuminates. First, near-threshold-width theory can explain that channels widen—via shear stress above the threshold to mobilize their bank materials—but not how they narrow. Therefore, existing equilibrium-width theory is only half of a true, balanced equilibrium solution to Equation 2: some way to describe and parameterize channel narrowing is required. Second, existing theory requires that a dominant channel-forming discharge of water be prescribed. If this is simply picked from the historical hydrograph, the lack of any mechanism for channel narrowing would require that river channels attain the width of their largest past flood. Although some glacial outburst-flood channels do retain a longstanding memory of ancient extreme events due to the inability of subsequent flows to change these patterns substantially (though many develop "underfit" streams inset into these floodways Dury, 1964; Libby, 2018; Naito and Parker, 2020), rivers forced by meteoric hydrology typically return towards a persistent hydraulic geometry following large floods (Wolman and Gerson, 1978). Therefore, near-threshold equilibrium-width

https://doi.org/10.5194/egusphere-2026-1018
Preprint. Discussion started: 6 March 2026

theory is tested on observed channel bankfull width and depth under the assumption that rivers persistently evolve towards an equilibrium channel width. Though the data support such a conjecture, existing theory cannot by itself explain the full drivers for or trajectory towards this observed hydraulic geometry.

Additionally, this simple-seeming thought exercise invites imagination into solutions that imply bed-elevation change. One possibility is that channel widening self-amplifies. This can occur in sheetflow events, in which deposition within such shallow flows can fill existing topographic lows and push a channel to expand across its surface (e.g., Sheets et al., 2007). Conversely, narrowing may self-amplify: a channel that begins incising may cut down the most where the flow-induced shear stress is the greatest, forming an inset channel. Further narrowing during incision can deepen flows, increasing shear stresses on the bed and causing the channel to continue to incise faster than the banks can erode to allow the channel to widen (Schumm et al., 1984; Cluer and Thorne, 2014). Such changes in bed elevation can accompany or be coupled with channel widening and/or narrowing. Here, we do not address this coupling in order to develop the channel-width theory alone. Therefore, we will maintain our focus on the solutions that converge towards an equilibrium or quasi-equilibrium width in absence of other forcings.

3 Assumptions

We make eight assumptions in the following physical model and its derivation, each of which is discussed in turn below:

1. The cross-section occurs along a straight reach of river.
2. All bank erosion and deposition occurs across the whole height of a rectangular channel.
3. Sediment mobilized from the banks is efficiently flushed out of the river cross section.
4. Erosion rate is limited by the slower process among cohesive particle detachment and noncohesive clast mobilization.
5. Stabilization of deposited sediment occurs instantaneously (as opposed to having a lag time associated with vegetation and/or biofilm development).
6. Suspended-sediment concentration is uniform with depth.
7. Bank shear stress is a constant multiple (< 1) of bed shear stress.
8. Bed shear stress may be computed using the depth–slope product.

3.1 Straight channel segment

We solve for the widening rate of a straight segment of river channel. This straight-channel assumption simplifies the solution by allowing us to assume a symmetrical flow field and neglect variations associated with flow around a bend (e.g., Hooke,

https://doi.org/10.5194/egusphere-2026-1018
Preprint. Discussion started: 6 March 2026

1975). The direct result of this assumption is that both banks receive the same shear stress. Therefore, the channel-widening rate, $\dot{b}_{\mathrm{w}}$, is twice the calculated bank-erosion rate, $\dot{\varepsilon}_y$:

$$\dot{b}_{\mathrm{w}} = 2\dot{\varepsilon}_y. \tag{3}$$

Likewise, the channel-narrowing rate, $\dot{b}_{\mathrm{n}}$ is twice the calculated bank-deposition rate, $\dot{\delta}_y$:

$$\dot{b}_{\mathrm{n}} = -2\dot{\delta}_y. \tag{4}$$

Here, the negative sign converts a positive lateral deposition rate into a negative rate of channel width change.

We consider this straight-channel assumption to be somewhat flexible for two reasons. First, Parker et al. (2011) introduced river meandering as a width problem in an asymmetrical flow field. We would not expect to observe the exact same widths in this situation as we would under symmetrical flow conditions because stresses vary across a bend from the outer to the inner bank and both erosion and deposition are threshold-based processes. Nonetheless, the outer-bank–inner-bank stress coupling via channel width (Parker et al., 2011) suggests that a similar equilibrium width be maintained. Second, large data compilations (Phillips and Jerolmack, 2016; Métivier et al., 2017) show broad agreements regarding equlibrium bankfull channel width across a wide range of channel forms, though it is possible that channel planform may account for some of the not-insignificant variability about the trend.

3.2 Rectangular channel

We assume a rectangular channel cross section to simplify the flow and channel-widening calculations. This permits us to use a straightforward Manning-style relationship with a break when the water surface exceeds the channel surface and flows start to spill overbank (Section 6). Furthermore, it allows us to consider mass balances involved in channel widening or narrowing to always be proportional to bank heights (i.e., the vertical distance from the channel bed to the floodplain).

This geometry becomes unintuitive—and likely unrealistic—during times of lateral deposition and associated channel narrowing. In the model presented here, a fraction of the sediment passing to the bank forms stable vertical faces attached to the bank edges (Section 3.5). We conceptualize this as an approximation of vertical accretion into vegetated bar edges. In truth, the primary reason for this approximation is to simplify the numerics: By maintaining vertical channel walls, we are able to calculate channel width as a scalar quantity that depends on Cartesian boundaries. Considering that most river channels are much wider than they are deep (Trampush et al., 2014), we consider that this may not be a poor approximation, and that inaccuracies will be compensated at least in part through tuneable parameters (Section 5.1.4 and Equation 30). Indeed, the rectangular-channel assumption is commonly used in models of river morphodynamics (e.g., Blom et al., 2017; Naito and Parker, 2019).

3.3 Eroded sediment is removed

We further apply the simplifying assumption that sediment supplied from the eroding banks does not impact the channel geometry. For muddy banks, we assume that any flow capable of causing erosion should have a high enough shear velocity to

https://doi.org/10.5194/egusphere-2026-1018
Preprint. Discussion started: 6 March 2026

loft these grains into wash load. When considering eroding banks made of sand or gravel, we assume that these larger clasts roll towards the higher-shear-stress channel thalweg. Along this course, they will experience ever-increasing shear stresses, and their mobility will increase as a result. In this latter case, our assumption requires either that the lateral bed-material sediment input be much less than the downstream bed-material sediment discharge ($Q_{s,y} \ll Q_{s,x}$) or that the whole river be in a dynamic quasi-equlibrium of shifting channels and banks (e.g., active braiding).

3.4 Rate-limiting process

We assume that channels will widen at a rate governed by the slower of two processes: erosion of cohesive materials and entrainment of noncohesive clasts. Considering only the former implies that streambanks are composed of materials with effectively negligble submerged weight but with nonzero cohesion. Considering only the latter implies that the banks are composed of loose clasts, lacking any cohesive matrix. Considering both together simulates a system in which clasts are embedded in a cohesive matrix.

We use the slower of these as the rate-limiting process required to erode a unit distance into the channel bank. Intuitively, clasts embedded in cohesive mud cannot be entrained until that mud is removed. Likewise, fine sediments may be armored by a surface layer of coarser, and harder to move, material. Symbolically,

$$\dot{\varepsilon}_y = \dot{\varepsilon}_{y,c} \wedge \dot{\varepsilon}_{y,n}, \tag{5}$$

where subscripts c and n represent the purely cohesive and purely noncohesive channel-widening rates, respectively, and $\wedge$ indicates that the minimum of these two values on the right-hand side be chosen.

3.5 Instantaneous stabilization of deposits

We assume that all material deposited on the streambanks instantaneously takes on the bank properties. This is a simplifying assumption for a process of stabilization that may take time, for example, due to the establishment and growth of vegetation (Tal and Paola, 2007, 2010; Pollen-Bankhead and Simon, 2010; Nicholas, 2013; Smith et al., 2021) or the gradual development of "sticky" organic aggregates (e.g., biofilms) within the sediments (Smith et al., 2022; Wei and Yang, 2023). We knowingly ignore these time-dependent processes and implicitly lump their representation into bulk bank-material parameters in order to reduce the parameter set and input data required to simulate river-width dynamics (see Sections 5.1.4 and 5.2).

3.6 Vertically uniform suspended-sediment concentration

When considering suspended-sediment transport to the banks, we do not consider variations in sediment concentration with depth within the flow. This corresponds to a Rouse number $\ll 1$. During overbank flooding, this assumption results in an unweighted partitioning between sediments traveling overbank and those interacting with the channel banks (Section 5.1). Given a suspended-sediment grain size and assuming a Rouse-style profile, future versions of the model could be updated with relatively little effort to relax this assumption.

https://doi.org/10.5194/egusphere-2026-1018
Preprint. Discussion started: 6 March 2026

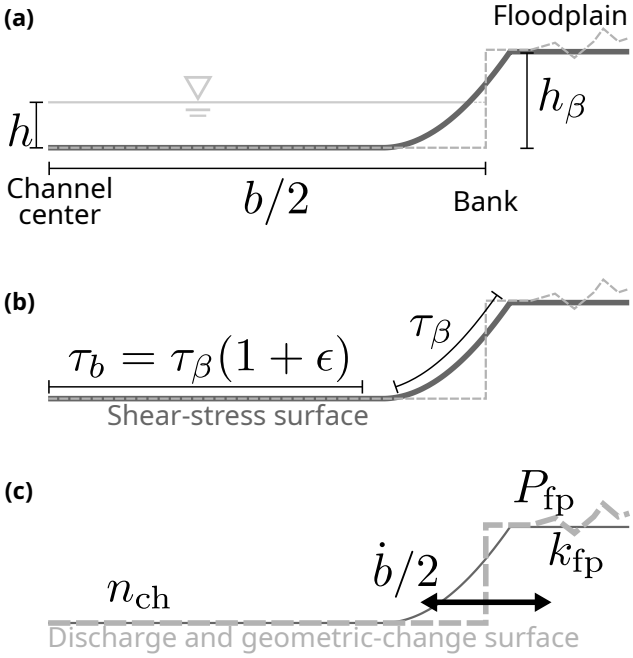

Figure 5. Variables involved in channel cross-sectional evolution. **(a)** Channel geometry. The curved bank-cross-sectional geometry provides a constant ratio between the near-bank shear stress and the stress required for the initiation of bank-gravel motion (Parker, 1978a), and a generally analogous relationship empirically holds true for sand-bed channels with banks of cohesive mud (Dunne and Jerolmack, 2020). At the same time, a rectangular geometry is input into depth–discharge relationships and is used for our simplified approach to channel-width adjustments. Deeper flows erode the bank faster, though this rate of increase diminishes after the flows become higher than the bank. Taller banks erode more slowly because they have more material to move per unit distance eroded. **(b)** Shear stresses at the bed (τ_b: nearer to the channel center) and along the banks (τ_β), and their relationship through ϵ (after Parker, 1978a). **(c)** Double-Manning parameters (Wickert et al., 2025) for flow velocity and stage–discharge relationships (Section 6) and channel-width adjustment. These include the in-channel Manning's n roughness parameter, n_{ch}; the power-law exponent for the overbank-flow depth–discharge relationship, P_{fp}; and the floodplain shape and inverse roughness coefficient, k_{fp}. Here, $\dot{b}$ is divided by two because we assume the half-channel depicted to be symmetrical.

3.7 Bank shear stress as a fraction of bed shear stress

We follow Parker (1978a) to convert bed shear stress, τ_b, into bank shear stress, τ_β:

$$\tau_\beta = \frac{\tau_b}{1+\epsilon}, \tag{6}$$

where $\epsilon \approx 0.2$. $\tau_\beta < \tau_b$ because resistance to flow can occur both along the channel bed and the channel bank in the near-bank region (Figure 5).

https://doi.org/10.5194/egusphere-2026-1018
Preprint. Discussion started: 6 March 2026

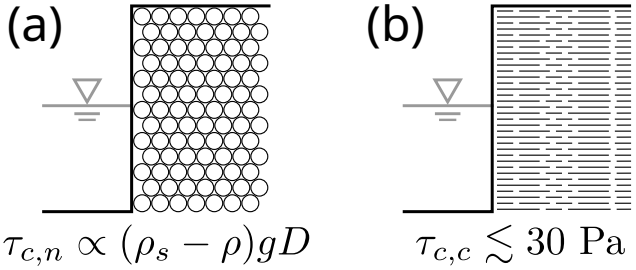

Figure 6. Bank strength sets the critical shear stress for particle detachment. **(a)** Noncohesive limit; $\tau_{c,n}$ stands for "shear stress: critical, noncohesive". Particle detachment occurs when the shear stress exceeds the critical threshold for particle entrainment, as provided by the Shields parameter (Equation 10). **(b)** Cohesive limit; $\tau_{c,c}$ stands for "shear stress: critical, cohesive". The critical stress to detach particles from a cohesive bank can vary. We found values $\lesssim$30 Pa in our literature review of soil and alluvial-stream materials (Table 1). In the present work, we consider widening rate to be associated with the slower between cohesive and noncohesive properties. If a bank has only cohesive mud, for example, this distinction is trivial. For a clast-supported gravel–mud mixture, the bank may be held stably by the weight of the gravel until it starts to mobilize, which is commonly more rapid than cohesive erosion (via the k_d parameter: Equation 8), at which point the slowness of the mud to erode sets the new limit on lateral erosion rate.

3.8 Bed shear stress from the depth–slope product

The computer program to solve for channel-width evolution (OTTAR: Wickert, 2026) computes basal shear stress by assuming normal (i.e., steady, uniform) flow. This permits shear stress on the channel bed to be solved using the depth-slope product:

$$\tau_b = \rho g h S, \tag{7}$$

where τ_b is the basal shear stress, g is gravitational acceleration, h is flow depth, and S is channel slope. By using flow depth, h, for shear stress, we assume that the channel is much wider than it is deep; analyzing bankfull widths from a global river data set (Trampush et al., 2014) indicates that the mean bankfull width-to-depth aspect ratio of rivers is 22. By using S, we are applying the small-angle approximation—that is, $S \equiv \tan\alpha \approx \sin\alpha$, for a downstream channel slope angle of α.

4 Widening

Alluvial river-channel widening is inhibited by streambank resistance to erosion. Here we consider two major erosional processes: (1) particle detachment from cohesive streambanks and (2) entrainment of noncohesive clasts (Figure 6). Following the arguments in Section 3.4, erosion and associated channel widening proceed at the slower of these two rates (Equation 5). An important implication here is that the weight of gravel clasts may set a channel's ultimate width, consistent with the work of Parker (1978a), but the erodibility of cohesive interstitial material can determine the rate at which the river approaches this equilibrium width.

https://doi.org/10.5194/egusphere-2026-1018
Preprint. Discussion started: 6 March 2026

4.1 Cohesive bank erosion

Cohesive streambanks erode through both small-scale particle detachment and larger scale mass wasting (e.g., Zhao et al., 2022). Mass-wasting events topple blocks into the river, which must be removed in order for the river to widen (Thorne and Tovey, 1981; Eke et al., 2014a, b). In streams with vegetated banks, these blocks may scale in size with tree presence and root structure (Pizzuto et al., 2010). Once blocks have fallen, they are removed via gradual detachment of their constituent cohesive particles. Therefore, we consider particle detachment to be the rate-limiting step for river-channel widening via cohesive streambank erosion.

The rate of erosion of cohesive materials due to particle detachment may be modeled as a power-law function of shear stress (Partheniades, 1965):

$$\hat{\dot{\varepsilon}}_{y,c} = \begin{cases} k_d \left(\tau - \tau_{c,c}\right)^a & \text{if } \tau > \tau_{c,c} \\ 0 & \text{otherwise} \end{cases}. \tag{8}$$

Here, $\hat{\dot{\varepsilon}}_{y,c}$ is the lateral erosion rate through cohesive materials, with the hat denoting that this is for a unit material thickness that we assume to equal the flow depth; this definition will become important when considering the fraction of the bank height against which the flow is actively performing geomorphic work. k_d is an empirically determined erosion coefficient; we use subscript d as a mnemonic for "detachment". τ is the applied shear stress, and $\tau_{c,c}$ is the critical shear stress at which particle detachment (and hence, erosion); "c,c" stands for "cohesive" and "critical" (see Figure 6). Although the material being eroded is commonly a porous medium, we follow convention in not invoking porosity into this equation, and therefore lump it implicitly into the k_d term. Likewise, any consideration of a mixture of cohesive and noncohesive material is contained within k_d. Khanal et al. (2016) demonstrated that a linear theory can fit observed erosion rates in rills and streambanks, so from a practical and simplifying standpoint, we invoke $a = 1$.

Next, we consider the fact that erosion occurs across the submerged portion of the bank. We assume symmetrical flow within a rounded but near-rectangular channel whose width is much greater than its depth and whose highest velocity occurs at the water surface in the centerline of the channel (Figure 5). Kean et al. (2009) demonstrated both theoretically and experimentally that the shear stress applied to the bank, τ_β, remains approximately constant with depth so long as the channel does not contain any sharp corners, which are uncommon in natural channels. We consider a uniform τ_β (which takes the place of τ in Eq. 8) across a flow depth h that is in contact with a bank of height h_β.

Combining the depth across which water-induced shear stress affects the bank with the aforementioned linear-erosion assumption, we write an equation to relate flow depth and bank height to lateral rate. For expediency, we drop the trivial case of $\dot{\varepsilon}_y = 0$ when $\tau_\beta < \tau_{c,c}$.

$$\dot{\varepsilon}_{y,c} = \begin{cases} k_d \frac{h}{h_\beta} \left(\tau_\beta - \tau_{c,c}\right) & \text{if } h < h_\beta \\ k_d \left(\tau_\beta - \tau_{c,c}\right) & \text{otherwise.} \end{cases} \tag{9}$$

When water flow depth is less than bank height (the first case), then lateral erosion occurs only along the depth of the contact of the flow and bank. When the flow goes overbank, erosion continues to occur only over the maximum possible distance—the

https://doi.org/10.5194/egusphere-2026-1018
Preprint. Discussion started: 6 March 2026

channel depth. We neglect the cross-channel bank slope because we are concerned with the lateral (i.e. y-directed) erosion: a cross-channel slope adds additional distance that must be eroded at precisely the same rate as it adds additional stress along-bank-integrated stress to perform this erosion.

If the erosion is through toppled blocks of bank material—or collapsed material from higher bluffs or terraces (e.g., Malatesta et al., 2017)—the state of stress on this collapsed material may not be exactly comparable to the geometry presented in Figure 5a and applied in Equation 9. In lieu of consiering the specific geometry and stress field, we accommodate this through a field-calibrated k_d, under the assumption that a given bank or bluff geometry should provide, on average, similar (in space and time) patterns and geometries of mass-wasting-generated material to the channel. Furthermore, we expect this factor to be small: Changes in the applied stress should vary with the ratio of bank height to post-failure block height (a factor of a few), which is small compared to potential variability in bank-material erodibility (several orders of magnitude: L. A. Clark and T. M. Wynn, 2007).

4.2 Noncohesive bank erosion

The approach to noncohesive bank erosion is largely analogous to that for cohesive bank erosion. We compute bank erosion rate via sediment entrainment as a linear function of excess Shields stress,

$$\tau^* = \frac{\tau}{(\rho_s - \rho)gD}, \tag{10}$$

above a critical value, τ_c^*. Here, ρ_s is sediment density, ρ is water density, g is gravitational acceleration, and D is the particle grain size; median grain size, D_{50}, is often used as a representative single-value surrogate for D, and this is what we implement here. Common values for the critical Shields stress (incipient motion) for gravel in water include 0.06 (Shields, 1936), 0.03 (Parker, 1990), and 0.0495 (Wong and Parker, 2006).

We next consider the rate of noncohesive-material entrainment. Lajeunesse et al. (2010, Fig. 5) show experimentally that the areal fraction of bed-load particles in motion increases linearly with excess Shields stress times 3.6±0.2 (see Equation 28). For a constant bed-load sediment concentration, new particles must be entrained when an in-motion particle is disentrained. Therefore, the entrainment rate must be inversely proportional to the time the particles spend in transit, Δt_m (where the m stands for "moving"), given by particle settling time (Lajeunesse et al., 2010, their Eq. 28):

$$\Delta t_m = (10.6 \pm 0.7)\sqrt{\frac{D}{[(\rho_s - \rho)/\rho]\, g}}. \tag{11}$$

Converting this entrainment rate into an erosion rate further requires a length scale of erosion into the bank, which should be proportional to the diameter of an entrained grain.

Combining these factors yields an equation with a similar functional form to that for cohesive erosion (Equation 9), but with an additional dependence on grain size and k_E as a coefficient for the efficiency of sediment entrainment. Taking mean values

https://doi.org/10.5194/egusphere-2026-1018
Preprint. Discussion started: 6 March 2026

Table 1. Value estimates or ranges for select variables. All units SI. Those values without references are coefficients specific to this work that were estimated by the authors. The best-fitting parameters for the four test rivers in our study (Table 2 fall within these ranges: $\tau_{c,c}$).

Variable	Value(s)	Reference
ϵ	0.2	Parker (1978a); Dunne and Jerolmack (2020)
$\tau_{c,c}$ (*in situ*)	0–30 Pa (for cohesive sediment banks)	Dunn (1959); Julian and Torres (2006); Simon et al. (2011); Daly et al. (2013); Daly et al. (2015a)[a]; Khanal et al. (2016)[a]; Konsoer et al. (2016); Dunne and Jerolmack (2020)
$\tau_{c,c}$ (lab)	0.5–10 Pa	Moody et al. (2005)[b]; Dunne et al. (2022)[c]
k_d (*in situ*)[d]	1–200$\times 10^{-6}$ m / (Pa s)	Daly et al. (2013); Khanal et al. (2016)[a]
τ_c^*	0.03–0.06; Default: 0.0495	Shields (1936); Parker (1990); Wong and Parker (2006)
k_E	>0–1	–
f_ς	>0–≈1	–
k_n	>0–1	–

[a] Iterative method
[b] Using data from Daly et al. (2015b)
[c] Hillslope soils from natural settings
[d] Varying sand–clay mixture from 0% to 100% clay
[e] Simon et al. (2011) empirically determined that $k_d \approx 1.62\tau_{c,c}^{-0.838}$, which may assist in parameter estimation

as representative of the distributions found by Lajeunesse et al. (2010),

$$\dot{\varepsilon}_{y,n} = \begin{cases} 3.6k_E \frac{h}{h_\beta}\left(\tau_\beta^* - \tau_c^*\right)\frac{D}{\Delta t_m} & \text{if } h < h_\beta \\ 3.6k_E\left(\tau_\beta^* - \tau_c^*\right)\frac{D}{\Delta t_m} & \text{otherwise.} \end{cases} \tag{12}$$

Here k_E is an efficiency parameter that exists in the range $0 \leq k_E \leq 1$. It scales inversely with the number of "hops" (individual transport events) required to fully remove a bed-load grain from the near-bank region. It may also serve as an imperfect proxy for the effects of lateral channel-bank slopes (Parker, 1978a) and sediment-grain interlocking (Masteller and Finnegan, 2017) on the threshold for grain entrainment.

To aid intuition in understanding the relationships between the variables, we expand the Shields stress and Δt_m for the case in which $h < h_\beta$. In particular, this shows that noncohesive erosion rate scales as $1/\sqrt{D}$:

$$\dot{\varepsilon}_{y,n} = 0.34k_E \frac{h}{h_\beta}\frac{\tau_\beta - \tau_{c,n}}{\sqrt{\rho(\rho_s - \rho)gD}} \tag{13}$$

Here, $\tau_{c,n} = \tau_c^*(\rho_s - \rho)gD$ is the dimensional critical shear stress required to initiate sediment motion; the "n" stands for "noncohesive", but is not included in the τ_c^* symbology to maintain a standard way of writing the Shields stress variable.

https://doi.org/10.5194/egusphere-2026-1018
Preprint. Discussion started: 6 March 2026

5 Narrowing

Channel narrowing due to bank deposition has been studied less than channel widening due to bank erosion (cf. Güneralp et al., 2012, Section 4.2). Prior studies indicate that channels can narrow through vegetation growth and encroachment on bars (e.g., Gran and Paola, 2001; Tal and Paola, 2010; Naito and Parker, 2019) as well as net sediment transport towards the banks via turbulent diffusion (mechanisms described by Parker, 1978b). Figure 7(b) depicts the conceptual model of this turbulent diffusion alongside some of the key associated variables.

We choose to incorporate both net sediment transport towards the bank and factors such as vegetation that can help to trap and hold sediment. The former is necessary to complete a consistent volume-balance approach to channel-width dynamics via both narrowing and widening. We represent the latter through coefficients that we describe below. These parameterize vegetation trapping and bank stabilization, but without the time lags and resultant hysteresis—such as for plant or biofilm growth—that should result when considering such biological processes more mechanistically.

To simulate channel narrowing, we include distinct but related expressions for suspended-load and bed-load transport to the banks. Whereas channel widening occurred at the pace set by the slower, rate-limiting process between cohesive-material detachment and noncohesive-sediment entrainment, channel narrowing rates are given by the sum of both of the processes simulated here. This is because both suspended load and bed load can deposit simultaneously, both contributing to bank deposition and channel narrowing. Symbolically,

$$\dot{\delta}_y = \dot{\delta}_{s,y} + \dot{\delta}_{b,y}. \tag{14}$$

Here, the character δ is chosen as a mnemonic for "deposition", subscript y indicates that this deposition is in the cross-channel direction, and subscripts s and b indicate narrowing due to suspended load and bed load deposition, respectively.

5.1 Turbulent diffusion of suspended sediment

To simulate river-channel narrowing through lateral deposition of suspended load, we invoke turbulent diffusion of sediment from the channel center towards the channel banks. In the case of suspended load, this diffusion is an apt phenomenological description of the net lateral sediment flux, $\hat{q}_{s,s,y}$, driven by turbulent eddies. The $\hat{}$ indicates that this is a true flux (units of length per time) rather than the typical depth-integrated flux used in sediment-transport equations. We describe lateral suspended-sediment sediment transport through a generalized diffusion relation:

$$\hat{q}_{s,s,y} = -K_{E,y}\frac{\mathrm{d}c_{s,s}}{\mathrm{d}y}. \tag{15}$$

From right to left, $c_{s,s}$ is the concentration of sediment suspended in the flow and $K_{E,y}$ is eddy diffusivity (see Section 5.1.3).

To convert lateral suspended-sediment transport into channel-narrowing rate, $\dot{\delta}_{s,s,y}$, we include several additional terms:

$$\dot{\delta}_{s,y} = -\frac{f_\varsigma}{1-\lambda_p}\frac{(h \wedge h_\beta)}{h_\beta}\hat{q}_{s,s,y} \tag{16}$$

λ_p is the porosity of the banks (λ_p), which acts to amplify narrowing because streambanks comprise both grains the void space between them. f_ς parameterizes the "stickiness" of the banks, which represents the presence of surfaces to which the

https://doi.org/10.5194/egusphere-2026-1018
Preprint. Discussion started: 6 March 2026

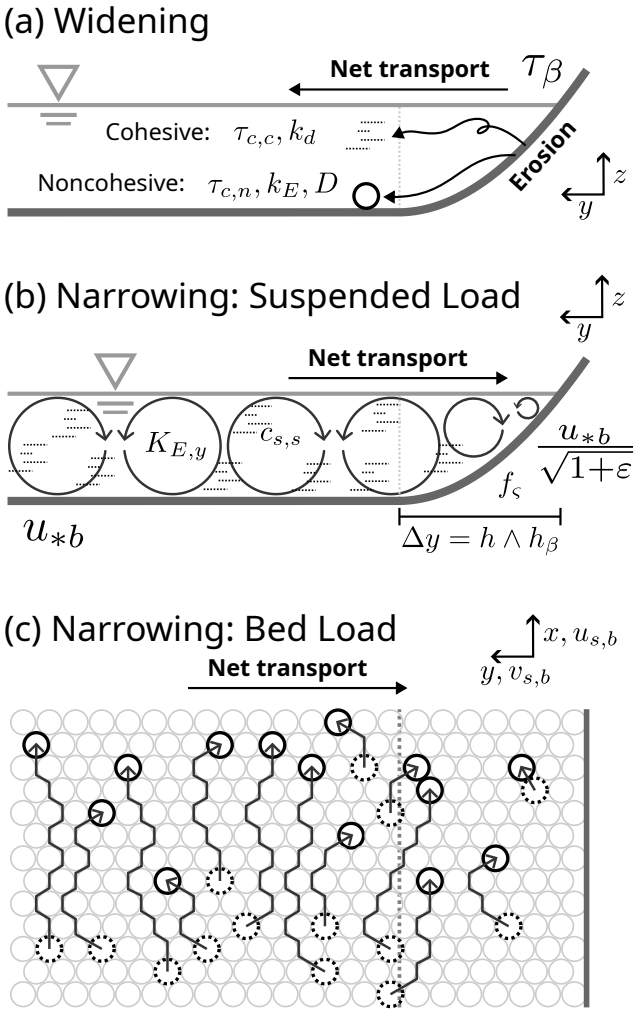

Figure 7. Mechanisms of river-channel widening and narrowing. Dark gray line: bed and bank. Medium gray line: water surface. Light gray dotted line: boundary of near-bank region. **(a)** Channel widening resulting from shear stress exerted on the bank, τ_β, in excess of a critical shear (cohesive: $\tau_{c,c}$) or Shields (noncohesive: $\tau_c^* = f(\tau_{c,n}, D)$ stress for particle entrainment. Sediment may be entrained as suspended load (dotted horizontal lines). It may also be entrained as bed load (black circle), which slides or rolls down the bank and into the middle of the flow. Entrainment rate increases with k_d and k_E for cohesive and noncohesive sediments, respectively; these relate to bank composition, structure, and geometry, as well as sediment-transport directions and rates. **(b)** Channel narrowing resulting from suspended-sediment diffusion from the channel center (higher concentration) towards the bank (lower concentration), across a distance Δy, and modulated by bank "stickiness" (entrapment efficiency: f_ς). Sediment concentrations are proportional to shear velocity, u_*. **(c)** Channel narrowing from net bed-load transport from zones of higher bed-load concentration and velocity (towards the channel center) to those of lower concentration and velocity (towards the bank). Bulk diffusive behavior results from the dynamics of the near-bed flow field and particle–particle collisions.

https://doi.org/10.5194/egusphere-2026-1018
Preprint. Discussion started: 6 March 2026

suspended sediment could adhere and/or locations in which it could become trapped and stabilized (section 5.1.4). Grain-size effects of sediment concentration (see below) are lumped into f_ς: this is likely to be a field-calibrated parameter, so although preemptively lumping these terms may obscure some clarity of process, it also prevents any unnecessary sense of a need to characterize suspended-load grain size. Nonetheless, we recommend that future process-specific approaches separate these components. The $(h \wedge h_\beta)$ term indicates that any suspended sediment above the height of the banks is considered to flow onto the floodplain – and hence, out of the domain of our model – and does not affect channel width directly. The linear relationship with flow depth above the bank height indicates that we assume a uniform vertical profile of suspended sediment (see Section 3).

5.1.1 Sediment concentration

We compute suspended-load sediment concentration following Rubin and Topping (2001, Equation 2), who show that

$$c_{s,s} \propto u_*^J D_{50}^K, \tag{17}$$

where $c_{s,s}$ is the suspended-load sediment concentration, $u_* = \sqrt{\tau/\rho}$ and D_{50} is median grain size of the sediment on the bed. For poorly sorted sand-bed rivers, with or without dunes, Rubin and Topping (2001, Table 1) show that $J = 3.5$ and $K = -1.5$. Well-sorted sands produce the pairs $J = 3.5$, $K = -1.5$ (without dunes) and $J = 5.0$, $K = -3.0$ (with dunes). Applying a similar analysis to the Engelund and Hansen (1967) formula gives $J = 4$, $K = -1$.

Here and in our model code (Wickert, 2026), we use $J = 3.5$ because this is the most common scaling found by Rubin and Topping (2001), and that which Dean et al. (2022) implemented through study of a natural sand-bed river. Furthermore, we assume that bed-material D_{50} remains constant within a reach, and therefore absorb the D_{50}^K term into the proportionality. Doing so is also important because the analysis by Rubin and Topping (2001) was only for sand-bedded rivers in which bed material may be lofted into suspension and thereby exchanged with the bed. Because we also consider gravel-bed rivers that may nonetheless contain finer sediments, the physical basis for connection between bed-material grain size and suspended-sediment concentration may be weakened or lost. In this case, the D_{50}^K term might not exist, but persistent conditions across a river reach should maintain a proportionality with shear velocity.

5.1.2 Concentration gradient

With these sediment-concentration formulations in hand, we next aim to find the concentration gradient required by Equation 15. Following our rectangular-channel assumption and the approximately uniform shear stress outside of the near-bank region (Parker, 1978a), we build a linear finite-difference approximation of the near-bank sediment-concentration gradient,

$$\frac{\mathrm{d}c_{s,s}}{\mathrm{d}y} \approx \frac{\Delta c_{s,s}}{\Delta y}. \tag{18}$$

The middle region of the channel, within which the influence of bank drag is negligible, has approximately uniform flow and sediment-transport conditions, and therefore, experiences an approximately uniform bed shear stress, τ_b, and shear velocity, u_{*b}. The near-bank region, defined as the zone in which flow is influenced significantly by bank drag, experiences a shear

https://doi.org/10.5194/egusphere-2026-1018
Preprint. Discussion started: 6 March 2026

stress on the channel walls τ_β and corresponding shear velocity $u_{*\beta}$, which are less than τ_b and u_{*b}, respectively, due to the partitioning of drag across both the bed and the bank. This remains the case until flows go overbank, at which point we approximate additional water thickness atop the channel to no longer be affected by substantial drag from the banks.

Following both this reasoning and the experimental and theoretical findings of Kean et al. (2009), we consider the width of the near-bank region to be defined by one flow depth when the flow is below the height of the banks, and to be equal to the bank height when the flow is deep enough to be able to travel overbank,

$$\Delta y = h \wedge h_\beta \tag{19}$$

With this distance in hand, we next must define the concentration gradient. We do so by converting equation 6 to an equivalent relationship for channel-center vs. near-bank shear velocity. For $h \leq h_\beta$,

$$u_{*\beta} = \frac{u_{*b}}{\sqrt{1+\epsilon}}. \tag{20}$$

Directly following from this and our proportionality based on Equation 17, we may write,

$$\Delta c_{s,s} \propto u_{*\beta}^{7/2} - u_{*b}^{7/2} \tag{21}$$

$$\propto \left[\left(\frac{1}{1+\epsilon} \right)^{7/4} - 1 \right] u_{*b}^{7/2}, \tag{22}$$

meaning that the difference in suspended-sediment concentration from the near-bank to the open-flow regions of the channel, $\Delta c_{s,s}$, is a strongly nonlinear function of shear velocity. This can be extended to all flow depths by noting that the water that lies above the banks experiences a more similar amount of drag above the channel center and close to the channel margins. Therefore, the overbank portion of the water column should not play a leading role in driving the shear-stress differentials that produce gradients in suspended-sediment concentration. Using the depth–slope product (equation 7) and definition of shear velocity we can then define this concentration gradient in terms of constants and measurable geomorphic variables,

$$\Delta c_{s,s} \propto g^{7/4} \left[\left(\frac{1}{1+\epsilon} \right)^{7/4} - 1 \right] S^{7/4} (h \wedge h_\beta)^{7/4}. \tag{23}$$

5.1.3 Eddy diffusivity

The eddy diffusivity ($K_{E,y}$) describes the rate of turbulent mixing within a flow, and therefore scales the net lateral sediment motion towards the banks via the suspended-sediment-concentration gradient. Both Parker (1978b) and Deng et al. (2003) note that lateral eddy diffusivity should scale with shear velocity (u_*) and flow depth. Parker (1978b) indicates that these should relate to eddy diffusivity by a factor of 0.13, whereas Deng et al. (2003) use data from Rutherford (1994) to suggest a factor of 0.16. We choose the former to be consistent with prior sand-bed river research, but note no other basis for this preference.

$$K_{E,y} = 0.13 u_{*b} h. \tag{24}$$

https://doi.org/10.5194/egusphere-2026-1018
Preprint. Discussion started: 6 March 2026

5.1.4 Bank "stickiness"

Not every grain of suspended sediment that touches the channel walls will remain there, and so we define a "stickiness" parameter, f_ς, which describes the fraction of the lateral sediment flux that adheres to the banks. In physical terms, f_ς can be thought of as a combined trapping efficiency and holding efficiency. Trapping may occur, for example, through vegetation intercepting sediment (Davies-Colley, 1997; Allmendinger et al., 2005; Parker et al., 2011) or within stable pits among sets of grains (Beschta and Jackson, 1979). The holding component describes how well the grains will stay in place rather than being quickly re-eroded. This "holding" could relate, for example, to biofilm development (Wei and Yang, 2023), plant-rootlet growth (Allmendinger et al., 2005), electrostatic cohesion among clay particles, and/or physical interlocking of grains on the bank (Smith et al., 2021, 2022).

By prescribing a single "stickiness" parameter, we are combining the instantaneous grain-trapping process with grain-holding process. In a real river, this grain-holding process may require time for biofilm development or root growth (cf. Eke et al., 2014a, who combine flow intermittency and vegetation towards a similarly conceptualized equation). Furthermore, bank stability may be reduced by vegetation die-off during a long drought, meaning that droughts punctuated by floods could be highly effective at generating wide channels (Schumm and Lichty, 1963). A more realistic approach to channel widening, therefore, could involve tracking changes in the bonding strength between grain and bank. This could cause, for example, a more erodible layer of not-yet-stabilized material along the banks to be remobilized by a large flood that shortly follows the depositional event that formed it. Because of the complexity of the linked biological and physical processes involved (cf. Nicholas, 2013), we use our single-scaling-constant approach and treat this channel narrowing as a process that does not require systemic memory.

Although unrelated to its namesake, the "stickiness" parameter also includes two terms associated with suspended-sediment concentrations. These are: (1) the constant of proportionality between suspended-sediment concentration and its drivers (Equation 17) and (2) any effects of absorbing this grain-size dependence (at least for rivers with fine enough grains to be brought into suspension) into this proportionality. As a result, f_ς may not be strictly bounded in the range (0,1], though in practice (Table 2), it seems to be.

5.2 Bed-load transport to banks

We build an expression to quantify bed-load deposition rate in the near-bank region, which together with lateral suspended-load transport sets the overall river narrowing rate (Equation 14). Grain-on-grain collisions deflect bed-load clasts from a direct path downstream (Charru et al., 2004; Lajeunesse et al., 2010). From these two experiments, we calculate an approximate ratio between downstream ($u_{s,b}$) and cross-stream ($v_{s,b}$) bed-load sediment transport,

$$\frac{u_{s,b}}{v_{s,b}} \approx 4. \tag{25}$$

In this calculation, we have assumed linear diffusion: although (Lajeunesse et al., 2010) noted superdiffusive behavior in cross-stream sediment, their data are well described by more straightforward Gaussian spreading.

https://doi.org/10.5194/egusphere-2026-1018
Preprint. Discussion started: 6 March 2026

Starting with this velocity ratio, we construct an expression for the cross-channel depth-integrated bed-load sediment flux towards the streambank, which here we take to be the positive y direction; q_{s,b,y^+}; this is equal and opposite to the flux in the negative y direction, and the sum of positive and negative fluxes (using the same coordinate-system conventions for both) should, in a uniform stress field, give net 0 lateral transport. Near the channel banks, however, applied shear stress drops, and we therefore expect a net transport gradient towards the banks, thus motivating our approach here.

To build an expression for lateral transport directed towards the bank, we combine particle velocity with the areal (x, y) concentration of bed-load particles in motion, $c_{s,b}$, and an appropriate vertical dimension. Sediment grains have a symmetrical distribution of lateral velocities, and therefore, half of the grains along a flowline will be moving towards the bank and half will be moving away from it. Therefore, we divide the concentration by two to give the concentration of grains moving towards the bank. For the vertical dimension, we use the mean height of a spherical grain on the bed, such that this value times the area of the sphere's circular cross section gives the grain's volume. When normalized by area, therefore, this mean height can provide the volumetric lateral sediment transport rate per unit downstream distance:

$$q_{s,b,y^+} = v_{s,b} \frac{c_{s,b}}{2} \frac{2}{3} D. \tag{26}$$

To provide an expression for the downstream sediment velocity, $u_{s,b}$, we restate the sediment-velocity relationship from Lajeunesse et al. (2010, their Eq. 26, 27) in terms of Shields stresses, rather than the more natural shear velocities, for congruence with the variable set applied in the remainder of this bed-load analysis:

$$u_{s,b} = (4.4 \pm 0.2) \sqrt{\frac{\rho_s - \rho}{\rho} g D} \left(\sqrt{\tau^*} - \sqrt{\tau_c^*} + 0.025 \right). \tag{27}$$

Here, τ^* can represent any Shields stress, and will be substituted for bank and bed stresses applied by the flow.

Lajeunesse et al. (2010) also measured the number of moving grains across a unit area of the channel bed. Assuming that these grains are spherical, thereby covering an area of $\pi D^2/4$ in the x, y plane, we use these experimental results to compute the fraction of the bed area covered by grains in motion,

$$c_{s,b} = (3.6 \pm 0.2) (\tau^* - \tau_c^*). \tag{28}$$

This equation is valid for $0 \leq c_{s,b} \leq 1$. If $\tau^* < \tau_c^*$, $c_{s,b} = 0$. If the calculated $c_{s,b}$ would be > 1, its maximum value remains held at 1. By doing this, we limit the thickness of the active transport layer to one grain diameter even as stress rises.

For typical values of $0.03 \leq \tau_c^* \leq 0.06$, the entire bed comes into motion at $4.6 \leq \tau^*/\tau_c^* \leq 8.2$. In contrast, Wilcock and McArdell (1993) found that complete mobility of sediment of a particular size class on a mixed-grain-size bed occurred when $\tau^*/\tau_c^* \approx 2$. This difference may result from grain-size mixtures: Lajeunesse et al. (2010) studied unimodal grain-size distributions, whereas the sand–gravel mixture of Wilcock and McArdell (1993) should enhance the mobility of the coarser grains. Effects of grain-size distributions on Shields-stress–entrainment relationships (i.e., hiding functions) may be incorporated into k_n in the narrowing case (Equation 30) and k_E in the widening case (Equation 12).

https://doi.org/10.5194/egusphere-2026-1018
Preprint. Discussion started: 6 March 2026

Together, Equations 25, 26, 27, and 28 define a lateral depth-integrated bed-load flux. For a chosen orientation (towards river left or towards river right, though again, we write this arbitrarily in the y-positive direction):

$$q_{s,b,y^+} = 1.3\sqrt{\frac{\rho_s - \rho}{\rho} g D^3}\,(\tau^* - \tau_c^*)\left(\sqrt{\tau^*} - \sqrt{\tau_c^*} + 0.025\right). \tag{29}$$

Equation 29 is one eighth of Equation 35 from Lajeunesse et al. (2010), approximated to two significant figures.

To compute the bed-load contribution to channel narrowing, we consider a flux across an imaginary plane separating the mid-channel region from the near-bank region. Bank-directed bed-load sediment flux across this plane will be a function of τ_b^*, and we write this as $q_{s,b,y^+}(\tau_b^*)$. Sediment flux directed towards the channel center across this plane is driven by the smaller τ_β^*, and we write this as $q_{s,b,y^+}(\tau_\beta^*)$. The difference between these two fluxes drives the portion of the channel-narrowing rate, $\dot{\delta}_{s,b,y}$, due to bed-load transport:

$$\dot{\delta}_{s,b,y} = \frac{k_n}{1-\lambda_p}\frac{1}{h_\beta}\left[q_{s,b,y^+}(\tau_b^*) - q_{s,b,y^-}(\tau_\beta^*)\right]. \tag{30}$$

Dividing by one minus the porosity $(1-\lambda_p)$ amplifies the depth-integrated sediment flux into bank-position change by accounting for interstitial spaces in the bank. Dividing by bank height, h_β, converts the areal rate of sediment supply to the bank into a linear rate of bank-position change.

The dimensionless constant, k_n, modulates the channel-narrowing rate. This constant, to be determined emprically, represents at least three factors that we have neglected or simplified: First, the true shear stress does not abruptly drop as a step function at a single plane (as we assumed for Equation 30), potentially affecting our flux estimates through random-walk dynamics. Second, the ability of the grain to find a stable pocket in the near-bank region where it can rest may prove to be important, depending on the sediment-surface configuration in the near-bank region. Third, vegetation establishment on bars and banks (e.g., Gran and Paola, 2001; Tal and Paola, 2010; Nicholas, 2013; Eke et al., 2014a) can stabilize sediment and contribute to channel narrowing. In sum, only a fraction of the bed-load sediment delivered to the near-bank region deposits on and remains on the channel banks. Therefore, $0 \leq k_n \leq 1$ (Table 1).

6 River discharge and shear stress

All four equations (9, 12 16, 30) describing mechanisms for channel widening or narrowing are functions of the shear stress exerted against the channel walls (Figure 8). Bed and bank shear stresses are set by river discharge, which modulates flow depths and velocities.

To convert discharge into bed and bank shear stresses, we apply a "double-Manning" approach to generate a flow-depth–discharge relationship that can accommodate changing hydraulic geometries. This approach combines the Manning (1891) equation for an approximately rectangular channel and region directly above it with a generalized power-law relationship for overbank flows that spread laterally (Wickert et al., 2025).

$$Q = \begin{cases} n_{\mathrm{ch}}^{-1} R_h^{2/3} S^{1/2} b h & \text{if } h \leq h_\beta \\ n_{\mathrm{ch}}^{-1} R_h^{2/3} S^{1/2} b h + k_{\mathrm{fp}} (h - h_\beta)^{P_{\mathrm{fp}}} & \text{otherwise.} \end{cases} \tag{31}$$

https://doi.org/10.5194/egusphere-2026-1018
Preprint. Discussion started: 6 March 2026

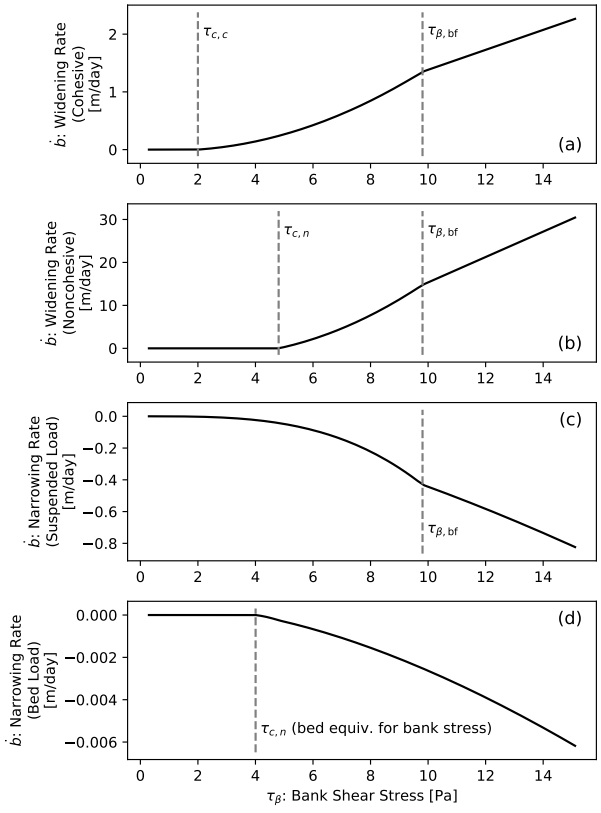

Figure 8. Channel-width evolution as a function of applied shear stress. $\tau_{\beta,\mathrm{bf}}$: bankfull shear stress applied to channel banks. $\tau_{c,c}$: critical shear stress for cohesive-material detachment. $\tau_{c,n}$ critical shear stress to mobilize noncohesive sediment. These numerical examples were produced with subsets of the following parameter set for each relevant plot: **(all)** Channel-width parameters: $h_\beta = 1.2$ m, $S = 10^{-3}$, $b_0 = 20$ m. Double-Manning parameters: $n = 0.025$ s/m$^{1/3}$, $k_{\mathrm{fp}} = 100$, $P_{\mathrm{fp}} = 1.75$. **(a)** $\tau_{c,c} = 2$ Pa, $k_d = 10^{-6}$, $f_\varsigma = 0$, $k_E = 0$, $k_n = 0$, D is undefined (widening occurs via cohesive-material erosion only). **(b)** $\tau_{c,c} = 2$ Pa, $k_d = 10^{-6}$ m / (Pa s), $f_\varsigma = 0$, $k_E = 0.1$, $k_n = 0$, D is undefined. **(c)** $\tau_{c,c} = 1$ Pa, $k_d = 0$ m / (Pa s), $k_E = 0$, $f_\varsigma = 1$, $k_n = 0$, $D = 6$ mm. **(d)** $\tau_{c,c}$ is undefined, $k_d = 0$ m / (Pa s), $f_\varsigma = 0$, $k_E = 0$, $k_n = 10^{-3}$, $D = 6$ mm.

Here, n_{ch} is Manning's roughness coefficient within the channel. k_{fp} and P_{fp} are the power-law coefficient and exponent, respectively, to describe floodplain flow. R_h, the hydraulic radius, is defined for a reectangular channel and the region above it as:

$$R_h = \frac{bh}{b + 2(h \wedge h_\beta)}. \tag{32}$$

We use data on river stage (water-surface elevation above a fixed datum) and discharge to calculate the free parameters in Equation 31 (e.g., roughness terms, floodplain-flow exponent). We assume that these remain constant even as the channel width evolves.

https://doi.org/10.5194/egusphere-2026-1018
Preprint. Discussion started: 6 March 2026

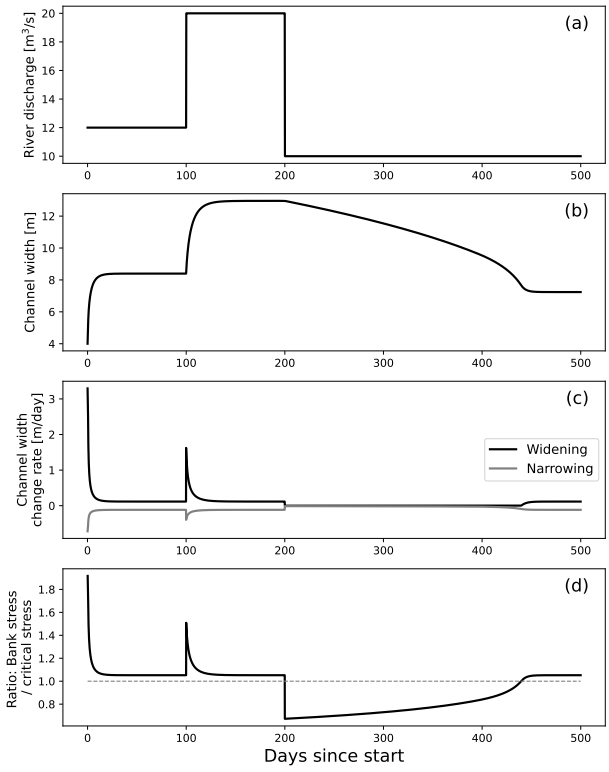

Figure 9. River widening and narrowing as simulated by simple synthetic time series of discharge inputs. When driven by a constant discharge, the set of equations presented here produce an equilibrium width close to the predictions of threshold-based theory Parker (1978a, for this gravel-bed case). The equilibrium shear stress is slightly higher than this threshold because our flux-based theory must enable enough erosion to balance the lateral depositional flux of sediment onto the banks. Channel-width (OTTAR) parameters: $h_\beta = 1$ m, $S = 10^{-2}$, $\tau_{c,c} = 5$ Pa, $k_d = 10^{-3}$, $k_E = 8 \times 10^{-3}$, $f_\varsigma = 5 \times 10^{-3}$, $k_n = 5 \times 10^{-3}$, $D = 6$ cm. Initial width (b_0): 4 m. Double-Manning parameters: $n = 0.025$ s/m$^{1/3}$, $k_{\text{fp}} = 100$, $P_{\text{fp}} = 1.75$. Time step: 0.1 days.

Equation 31 demonstrates that, for a given discharge, flow depth decreases as channel width increases. Through this mechanism, channel widening reduces bed and bank stresses, thereby reducing the bed and bank erosion rates. This hydraulic–geomorphic feedback enables the channel to smoothly and asymptotically approach and attain a stable width.

7 Schematic implementation

We first test our code and its stability through a schematic implementation (Figure 9) in which we prescribe a steady discharge that we first raise and then lower. Here, we see the channel widen from its too-narrow initial condition to equilibrate with the initial steady discharge over the course of several days, and again following the step increase in discharge on Day 100. Channel narrowing, in this example, takes place more slowly, but accelerates shortly after Day 400. The early phase of channel

https://doi.org/10.5194/egusphere-2026-1018
Preprint. Discussion started: 6 March 2026

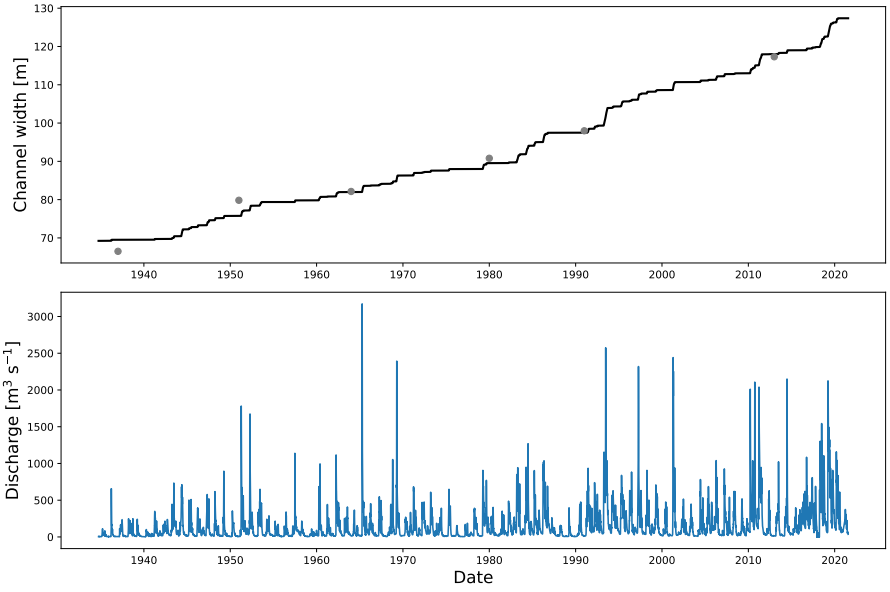

Figure 10. Minnesota River near Jordan, Minnesota, USA. Black line: modeled channel width. Gray points: measured channel width by Libby (2018).

narrowing is driven only by suspended-sediment diffusion towards the banks. As the channel narrows and shear stresses on the bed increase sufficiently to mobilize bed-material sediment, net bed-load diffusion towards the banks augments the net bankward suspended-load transport and accelerates the pace of channel narrowing.

In Figure 9(d), the equilibrium ratio of τ_β/τ_c is slightly greater than one. This differs slightly from the simpler erosion-limiting relationships of Parker (1978a) and Dunne and Jerolmack (2018) due to the small amount of erosion required to balance deposition on the banks. However, the numerical value of this offset fits easily into the range of observations: see Figure 2 for gravel-bed, gravel-bank rivers and Dunne and Jerolmack (2018) and Dunne and Jerolmack (2020) for sand-bed, mud-bank rivers.

8 Case-study applications

We compare the numerical implementation of our theory (OTTAR: Wickert, 2026) to data from four river systems: the Minnesota River (Minnesota, USA), the Cannon River (Minnesota, USA), Diamond Fork (Utah, USA), and Green River (Utah, USA). Case-study river systems were chosen to include sand-bed, mixed sand- and gravel-bed, and gravel-bed river reaches that are either narrowing or widening. By testing our theory on four sites that sample widening vs. narrowing and sand vs. sand and gravel, we demonstrate that our theory for transient river width evolution is generally applicable.

Our first step towards each of these implementations is to obtain basic data on each of the river study reaches. This includes information on bank height, channel slope, and bed-material sediment grain size (Table 2). Qualitative and/or quantitative

https://doi.org/10.5194/egusphere-2026-1018
Preprint. Discussion started: 6 March 2026

observations on the presence of cohesive banks and bank stability can help here as well, though for these implementations, we do not take field measurements of $\tau_{c,c}$ or k_d. In general, although such bank-strength measurements may be helpful, we expect there to be significant materials heterogeneity and hence, spatial variability, in bank resistance to erosion (Konsoer et al., 2016). Therefore, although a field measurement should provide guidance towards these parameters, model calibration (as is done here) remains recommended.

Second, we assembled hydrograph data (Table 2) from each reach of interest and relate river discharge to stage. To perform the latter, we apply the double-Manning approach (Wickert et al., 2025) to stage–discharge rating-curve data repeatedly measured at a known, stable cross section associated with the stream gauge and whose roughness and floodplain characteristics are similar to those of the study reach (Wickert, 2025b). We input a field-measured bank height alongside this stage–discharge relationship, h_β and compute the Manning's n roughness parameter and the floodplain power-law parameters (Table 2). These parameters then permit us to convert between discharge and river stage for variable river width.

Third, we obtained data on river-width changes over time. Some data were sourced from previous studies while other were generated for this study. The methods for extracting channel widths vary slightly by data source, though all are based on measurements from aerial photographs. Early measurements in the channel-width time series also serve as guides to select the initial width, b_0 (Table 2).

With this starting information in hand, we sequentially applied the Efficient Global Optimization method (EGO: Jones et al., 1998) and nonlinear least squares optimization method (NL2SOL: Dennis et al., 1981) to estimate the following parameter values by minimizing the root mean squared error between the measured and modeled river width at measurement time points:

b_0 initial channel width;

$\tau_{c,c}$ the critical shear stress to detach cohesive material;

k_d the associated detachment-rate coefficient for cohesive sediment;

k_E the entrainment coefficient for noncohesive sediment;

f_ς the "stickiness" coefficient for on-bank deposition of suspended sediment;

k_n the narrowing-rate efficiency coefficient via bed-load sediment.

The parameter estimation approach followed that used by Barnhart et al. (2020) and was implemented using the Dakota toolkit (Adams et al., 2020). The sequential optimization approach results in an initial parameter estimate using the EGO method that is subsequently refined using the NL2SOL method. Table 2 holds best-fitting values for each of these parameters at each of our river test sites. River-width data, input files for DAKOTA that document how the EGO and NL2SOL methods were configured, and associated code are available from Wickert and Jones (2026).

By applying our theory and its numerical implementation across this set of distinct river reaches, we test our claim that the theory is general. These successful tests, shown below, demonstrate that parameter sets exist that can reproduce the width dynamics of both sand- and gravel-bed river reaches. These indicate that the theory presented here is a plausible sediment-flux-based framework for transient channel-width evolution.

https://doi.org/10.5194/egusphere-2026-1018
Preprint. Discussion started: 6 March 2026

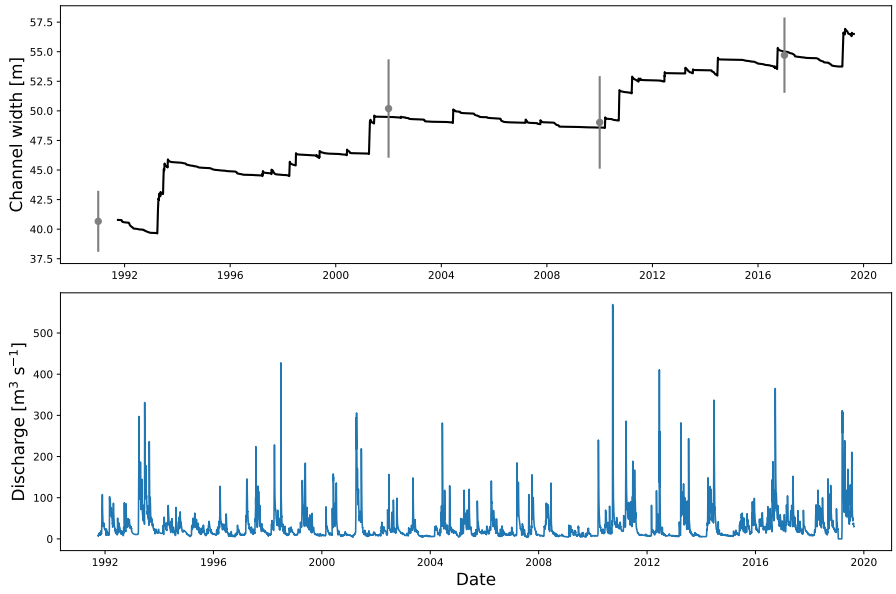

Figure 11. Cannon River at Welch, Minnesota, USA. Black line: modeled channel width. Gray points with error bars: measured channel width and 1-standard-deviation error.

8.1 Minnesota River

The Minnesota River is predominantly a sand-bed river that flows through western and central Minnesota and is a major tributary to the Mississippi River. The Minnesota River and its tributaries are adjusting to catastrophic drainage(s) of glacial lakes, predominantly Glacial Lake Agassiz, that occurred at the end of the last glaciation. As a result of the meltwater drainage, a valley was carved up to 70 m deep and up to several km wide in locations. Today, the valley is occupied by the underfit Minnesota River. Tributaries to the Minnesota River have observable knickpoints and knickzones that are progressing upstream through the watersheds. In addition, thousands of mass wasting events have been recorded on the steep valley margins, sometimes aided by undercutting by the laterally migrating river (Kohout2019, Swanson et al. 2019). As a result, there are naturally large sediment loads from the valley margins and distinct geomorphic zones in tributaries upstream and downstream of the knicks (Gran et al., 2009; Belmont et al., 2011a; Vaughan et al., 2017). In addition, recent climatic and land-use changes have led to increased streamflow in the last 50 years (Foufoula-Georgiou et al., 2015; Kelly et al., 2017; Pathak et al., 2017; Li and Quiring, 2021). These changes have led to bank and bluff erosion, increased sediment (turbidity) and nutrient loading, and ecological damage (Belmont et al., 2011a, b; Lenhart et al., 2013b; Lauer et al., 2017; Kelly and Belmont, 2018; Boardman et al., 2019; Hornbach et al., 2019)

We assembled data from the Minnesota River near Jordan, Minnesota, because of its long streamflow record. Channel width data for the Minnesota River come from Libby and Larson (2016) and Libby (2018), who compiled aerial photographs from 1937, 1951, 1964, 1980, 1991, and 2013. They hand-digitized the river banks at a 1:2000 scale, assessed total spatial error

https://doi.org/10.5194/egusphere-2026-1018
Preprint. Discussion started: 6 March 2026

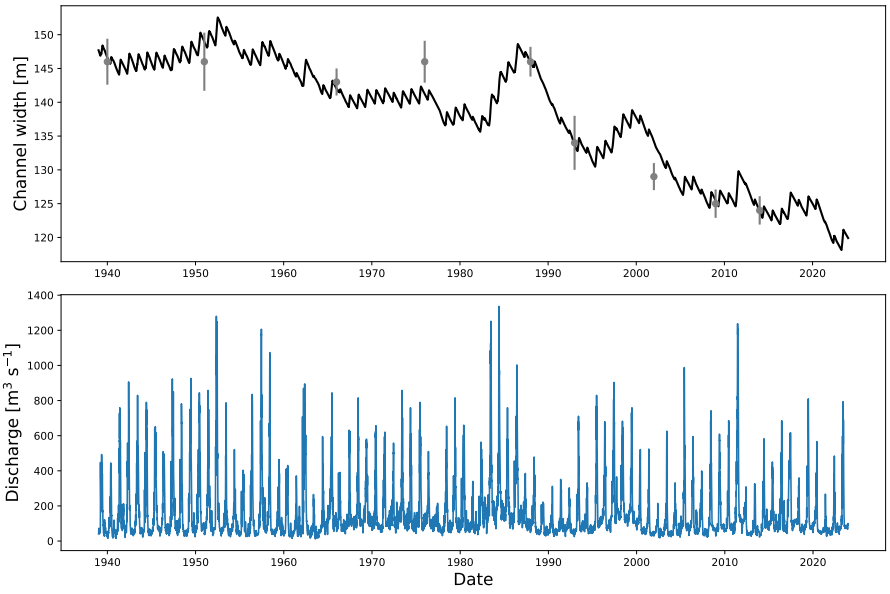

Figure 12. Green River at Fort Bottom, Utah, USA. Black line: modeled channel width. Gray points with error bars: measured channel width and 1-standard-deviation error from Walker et al. (2020).

following Lea and Legleiter (2016), and measured channel width using the NCED Planform Statistics Tool in ArcGIS Lauer (2006). Channel geometry data come from Kelly and Belmont (2018); Kelly et al. (2018); Kelly (2019), who extracted the height of banks from lidar, measured bed and water surface slope in the field using RTK GNSS, and measured bed-material grain size via bed samples at 8 sites throughout the lower Minnesota River.

Our best-fitting model closely matches the observed widening of the Minnesota River near its gauge at Jordan, Minnesota, USA (Figure 10). By testing the parameters associated with this best-fitting model (Table 2), we find that the river widens once its shear stress overcomes the cohesive strength of the banks ($\tau_{c,c}$ = 4.99 Pa). This stress is close to the bank stress exerted by a bankfull discharge (4.74 Pa). Once this cohesive strength is overcome, the rate of channel widening is controlled by the entrainment rate of the sand (i.e., the noncohesive particles) stored in the bank (K_E). Running counter to these widening trends, the river narrowing rate associated with this model is very small. This slow rate may be unrealistic: we calibrated the parameters to data from the Minnesota River, which is monotonically widening, and therefore acts as a poor constraint on channel-narrowing dynamics.

8.2 Cannon River

The Cannon River is a mixed gravel and sand bed river in southeastern Minnesota, USA. The western portion of the Cannon River watershed was glaciated during the most recent glacial period, but the eastern portion was not. Modern land use in the Cannon River watershed is 76% agricultural, with more agriculture in the western portion (DeZiel et al., 2014). Agriculture is

https://doi.org/10.5194/egusphere-2026-1018
Preprint. Discussion started: 6 March 2026

accompanied by artificial drainage in the form of ditches and tile drains, a system of subsurface pipes that enhance drainage in poorly drained soils. Based on county-wide data, roughly 45% of the total land area in the watershed was drained by ditches or tile drainage in 2022 (U.S. Department of Agriculture, National Agricultural Statistics Service, 2024). In addition to land-use changes that have altered hydrology, precipitation in southeastern Minnesota has increased over the last 50 years (Pathak et al., 2017). Climate and land-use change contribute to ongoing ecological concerns, including sediment and nutrient loading (DeZiel et al., 2014; Schottler et al., 2014; Wotzka and Watkins, 2016; Lenhart et al., 2013a).

Channel width for the Cannon River was measured on aerial photographs dating from 1938 to 2017 (Jones, 2024). Data collection on the Cannon River was motivated by a desire to understand regional differences in channel behavior driven by climatic and land-use change, given the large volume of work conducted on the Minnesota River and relative paucity of work on other rivers in the region. The channel planform was digitized at 1:2000 scale by a single operator and channel width was extracted via the Planform Statistics tool at 10 m intervals (Jones, 2024). For comparison with our model runs, we extract channel widths from near the Cannon River at Welch USGS stream gauge (05355200).

Like the Minnesota River, the Cannon River widens when the flow overcomes the critical shear stress to overcome bank cohesion, and it widens at a rate governed by the entrainment of clastic sediment (Figure 11). Unlike the Minnesota River case, however, the computed bank cohesion for the Cannon River (13.73 Pa) is comparable to the stress required to entrain the bed-material gravels (7.7 Pa). Furthermore, its best-fitting solution includes channel narrowing. As simulated, this narrowing occurs primarily through deposition of suspended sediment onto the banks, with the bed-load-deposition component of narrowing (Figure 7(c)) being negligible.

8.3 Green River

The Green River is a sand-bed river that crosses Wyoming, Colorado, and Utah. It is the largest tributary to the Colorado River; indeed, prior to 1921, its confluence defined where the Colorado River began (U.S. Congress, 1921). Due to damming, withdrawals, and climate change, the annual flow of the Green River decreased during the 20th Century, with a significant reduction after 1929 (Walker et al., 2020). Peak flows decreased in the mid-20th Century due to combined effects of climate change and the completion of Flaming Gorge Dam in 1962 (Allred and Schmidt, 1999; Grams and Schmidt, 2002; Walker et al., 2020). In addition, riparian plants, including non-native tamarisk (*Tamarix spp.*) have successfully colonized riparian areas along much of the Green River (Graf, 1978; Allred and Schmidt, 1999; Walker et al., 2020), impacting ecosystems, landscape function, and management Quigley (2013); Wehi et al. (2023). As a result of vegetation establishment and flow reduction, the Green River has significantly narrowed since the early 20th Century (Graf, 1978; Andrews, 1986; Allred and Schmidt, 1999; Grams and Schmidt, 2002, 2005; Grams et al., 2020; Walker et al., 2020).

Channel-width data for the Green River come from Walker (2017), who measured channel width from aerial photographs between 1940 and 2014 as part of a larger study on the timing and mechanisms of channel narrowing. Walker (2017) and (Walker et al., 2020) produced average channel widths at 1-km intervals by mapping polygons of the active channel and dividing channel polygon area by length. Channel-geometry data are compiled from (Walker et al., 2020, bank height), (Dean

https://doi.org/10.5194/egusphere-2026-1018
Preprint. Discussion started: 6 March 2026

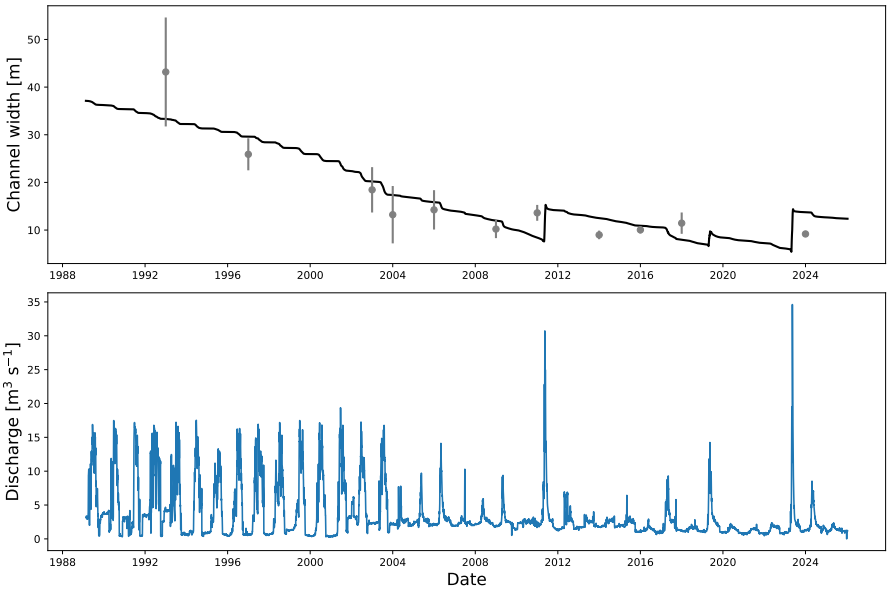

Figure 13. Diamond Fork River above Motherlode, Utah, USA: Reach defined by Jones (2018). Discharge record rescaled based from Diamond Fork above Red Hollow using the ratio of the drainage areas. Black line: modeled channel width. Gray points with error bars: measured channel width and 1-standard-deviation error.

et al., 2020b, channel slope), and (Dean et al., 2020a, median grain size). We compare measured and modeled channel width at river mile 43.81, near where Walker et al. (2020) evaluated stratigraphy within a floodplain trench.

To fit the data, we simulate dynamic widening and narrowing (Figure 12). Annual widening occurs during most years with the snowmelt flood. Narrowing occurs during the lower flow conditions later in the year. As above, widening occurs when the flow overcomes the critical shear stress from the cohesive forces binding the bank-material particles together. Once this stress is overcome, it proceeds at a pace proportional to the entrainment rate of the sandy bank-material sediments. Unlike the above cases, the narrowing rate is set by accretion of bed material – in this case, medium sand – to the bank.

8.4 Diamond Fork

Diamond Fork is a bedrock and gravel-bedded river in the Wasatch Mountains of central Utah, USA. Beginning in 1915, Diamond Fork and a tributary, Sixth Water Creek, were used to convey irrigation water for agricultural use. Irrigation deliveries greatly exceeded the natural summer flow regime, with the largest imported flows exceeding a 500-year flood at the headwaters and a 10-year flood at the outlet of Diamond Fork (Jones et al., 2023). These large flows, in concert with natural floods, caused channel widening throughout the Sixth Water/Diamond Fork system in the 20th Century. Reduced flows began in 2004 after the completion of a series of irrigation tunnels and pipelines. The new flow regime includes no large releases, but baseflows are elevated relative to the natural regime.

https://doi.org/10.5194/egusphere-2026-1018
Preprint. Discussion started: 6 March 2026

Channel width for Diamond Fork was measured on aerial photographs between 1939 and 2018 (Jones, 2018; Jones et al., 2023), extended for this study to 2024 and to include a single-thread reach just upstream of the Motherlode site. Airphotos were digitized at a 1:1000 scale by a single operator, and channel width for the photos was extracted via the Planform Statistics tool (Lauer, 2006; Lauer and Parker, 2008) and cmgo (Golly and Turowski, 2017) at 10 m intervals. Channel geometry data for the Diamond Fork were collected via lidar, RTK-GNSS surveys, and pebble counts (OpenTopography, 2018; Jones et al., 2021, 2023).

The Motherlode reach lies downstream of the stream gauge above Red Hollow, from which the discharge record comes. To create a discharge time series appropriate for this location and to encompass the period of narrowing, we used a two-step approach. First, we built a power-law fit between the gauging records Below Red Hollow (USGS-10149500, 1989–2001) Above Red Hollow (USGS-10149400, 2001–2026) using a period of gauge overlap in 2001. Using this fit, we projected the Below Red Hollow record into a continuous Above Red Hollow record spanning 1989–2026. Next, We followed the model-based scaling of Stout (2019) to project our longer-term Above Red Hollow record to the Motherlode reach.

The model fit to the Diamond Fork data captures the transition from narrowing to stability, but produces the lowest quality fit of the four reaches studied. The best fit approaches, but does not reproduce, the rapid narrowing and later stability of the channel. One reason behind this result could be that our model inversion imposed constant parameters whereas Jones et al. (2023) noted that vegetation expanded across the river system following the end of flow augmentation. This suggests that channel-geometry modeling may require a dynamic feedback with riparian vegetation. Indeed, physical experiments (Tal and Paola, 2007, 2010) and numerical models (Nicholas, 2013) already demonstrate the importance of vegetation in modulating river planform, including channel width.

9 Discussion

We developed a flux-based model for river-channel widening and narrowing. First, a time-series of river discharge is converted to a time-series of flow depth and shear stress using a dynamically adjusting double-Manning rating curve (Wickert et al., 2025). The shear-stress time series drives widening through bank-material entrainment and narrowing through diffusive net transfer of sediment towards the channel margins. When this transiently evolving model reaches steady state, channel width and associated shear stresses are close to those predicted by threshold bank-stress theory (Parker, 1978a; Dunne and Jerolmack, 2018). When applied to a set of hydrologically and geomorphically distinct river reaches, an optimization approach for parameter calibration minimizes misfits between model outputs and observed data. Here we consider the conceptual difference between flux-equilibrium (this model) and threshold-stress approaches, consider how the time-variable hydrograph forces a dynamic equilibrium with associated width variability, discuss applicability to sinuous channels, consider ecological influence on bank strength, and present implications for fluvial hazards.

https://doi.org/10.5194/egusphere-2026-1018
Preprint. Discussion started: 6 March 2026

9.1 Contrasting flux-equilibrium and threshold-based theories

Leading theories for the development of self-formed river channels indicate that they reach an equilibrium state in which the stress exerted on the banks is exactly equal to the stress required to erode the banks (Phillips et al., 2022). For cohesive stream-bank materials, this critical stress is $\tau_{c,c}$ from Equation 8 – the threshold for initiation of particle detachment associated with bank-material cohesion (the "sand-bed" case: Dunne and Jerolmack, 2018, 2020). For noncohesive stream-bank materials, this critical (dimensional) shear stress corresponds to the Shields stress (Equation 10) for initiation of particle motion (the "gravel-bed" case: Parker, 1978a).

Calling these river-width (and hence, boundary-stress) states an "equilibrium" requires, by definition, that drivers of change are balanced. In the case of alluvial river channels, this means that the flux of sediment away from the banks (erosion: channel widening) is balanced by the flux of sediment towards the banks (deposition: channel narrowing). The aforementioned theory includes the balance and the result, but not how it is attained. Popović et al. (2021) produced this balance of bank erosion and lateral sediment diffusion in the laboratory, generating channels in non-cohesive sediments whose bed Shields stresses were slightly above the threshold for motion, in agreement with theory (Parker, 1978a).

Here we simulate channel-width evolution using the same two processes observed by (Popović et al., 2021)—bank erosion and lateral sediment diffusion—and expand this approach to account for bed-load sediment, suspended sediment, and both noncohesive and cohesive bank materials. Furthermore, we simulate dynamic river-channel change and (dis)equilibrium via time-variable flow, which drives observed variability in river-channel width in the field (Phillips et al., 2024; Slater et al., 2019) as well as in our model outputs (Section 8). By reproducing width evolution of a diverse set of river channels, we demonstrate that our equation set is plausible. Perhaps more importantly, we show that, when forced with a constant discharge, our equation set and model can produce a static equilibrium that lies close to that of the Parker (1978a) theory (Figure 9).

9.2 Dynamic equilibrium

Flow variability forces real rivers towards dynamic equilibrium widths (Figure 9) that can vary substantially from those predicted by equilibrium-width theory (Parker, 1978a; Dunne and Jerolmack, 2018, 2020), corroborating field-based findings (e.g. Andrews, 1982; Pizzuto, 1994; Slater et al., 2019; Phillips et al., 2024). To investigate such variability and its impacts on channel conveyance capacity (Slater and Singer, 2013; Slater et al., 2015, 2019; Ahrendt et al., 2022), we drive the Green River by repeating its 1939–1969 hydrograph until the simulated river width converges to a dynamic steady state (Figure 14). After 3–4 cycles, the river width becomes statistically stationary, but retains significant annual and multi-annual variability. This variability in river width produces a 9.3% variance in bankfull discharge with respect to time-averaged mean bankfull discharge. This variability likewise may account for some amount of the variance between predicted and observed bankfull bank shear stresses (Figure 2).

https://doi.org/10.5194/egusphere-2026-1018
Preprint. Discussion started: 6 March 2026

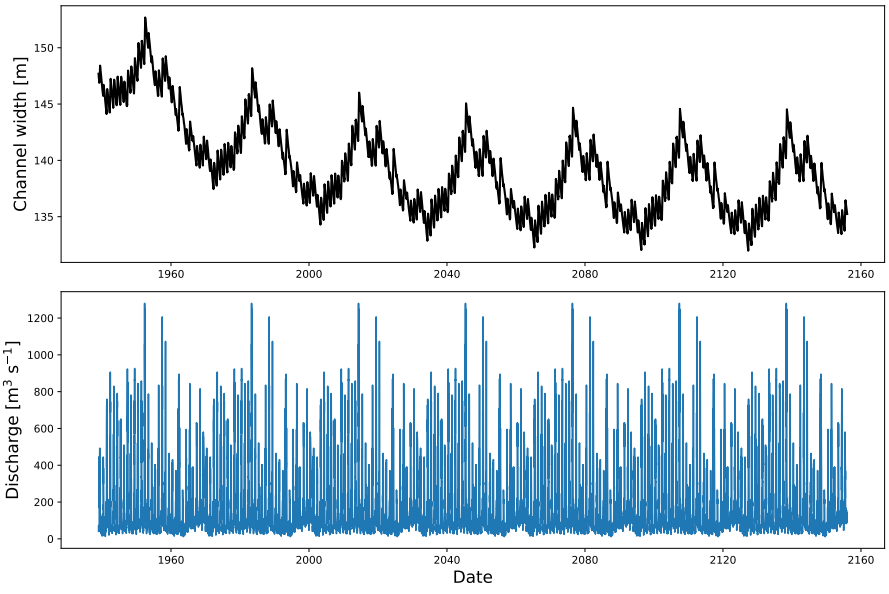

Figure 14. Dynamic equilibrium. Using the best-fitting model parameters for the Green River (Section 8.3; Table 2), we drive river-width evolution by repeating the 1939–1969 hydrograph seven times.

9.3 Straight and sinuous channels

Here we set up the stress distributions and flux balances for a straight channel: sediment-transport rates and channel-width evolution are symmetrical around a stationary channel centerline. We do so because the straight symmetrical channel permits us to analyze a single cross section without concern for lateral flow variations upstream or downstream. Its simple geometry also provides a natural starting point to address river-channel width dynamics that permits extension to more complex river-channel patterns.

Paradoxically, the symmetrical case presents a more complex solution to envision than do width dynamics along a meandering channel. Our theory for symmetrical channels requires that both channel walls be able to experience erosion and deposition simultaneously. In contrast, meandering rivers have been successfully modeled by prescribing that the outer banks of bends are purely erosional and that the inner banks (point bars) are purely depositional (Parker et al., 2011; Eke et al., 2014a; Naito and Parker, 2019, 2020). This asymmetry leads to channel migration as a direct result of this "lateral sediment pump" to solve channel-width dynamics. This one-way pump can be envisioned as a counterpoint to our symmetrical channel, and one that is ubiquitous in nature.

How might this case differ from our symmetrical model? Towards the depositional side of the channel: stress asymmetries and larger-scale flow patterns (both along the channel and secondary helical flow) may act to more effectively transmit sediment towards the point bar (Hooke, 1975; Dietrich and Smith, 1983, 1984), and perhaps via some advective transport component in addition to diffusion. Towards cut-bank erosion: channel curvature will allow flows to exceed the threshold stress for erosive

https://doi.org/10.5194/egusphere-2026-1018
Preprint. Discussion started: 6 March 2026

channel widening at lower discharges than in a straight channel. In sum: the effects of channel curvature serve to speed the rate of both channel widening and channel narrowing. Therefore, it is possible that the equilibrium states may differ, and it is likely that the rate at which sinuous rivers approach equilibrium widths is faster than straight rivers.

All of our calibrated field example rivers (Section 8) have meanders. Nonetheless, we are able to capture their dynamic evolution. Though we do not explicitly account for sinuosity in any of our parameters, sinuosity has the effect of altering erosional and depositional efficiency via stress asymmetry, as noted above. Functionally, tuning the parameters for efficiency of erosion and deposition can account for the effects of sinuosity.

9.4 Ecological change and bank-strength dynamics

In Section 3.5, we note our simplifying assumption that deposited material instantaneously takes on the properties of the stream bank, but that this neglects the real time-variable dynamics of ecological processes. The critical shear stress to overcome bank cohesion, $\tau_{c,c}$, and the cohesive-erosion-rate parameter, k_d, should begin as small values for new deposits and increase over time as vegetation (Libault and Pigay, 2002; Pollen-Bankhead and Simon, 2010) and biofilms (Wei and Yang, 2023) colonize new surfaces and grow. Such changes in the bank properties may likewise impact the bank "stickiness" (f_ς, its ability to catch and hold suspended sediment that impacts the banks) and the ability to trap and hold bed load along the bank (as represented within k_n).

In addition to time lags, climate and ecosystem variability also impact vegetation dynamics and bank stability. Schumm and Lichty (1963) note that periods of aridity followed by large floods can cause extreme river widening, such as the 12-fold increase in width of the Cimarron River (Kansas, USA) in their study, because vegetation weakening and die-off precedes the erosional event. Manners et al. (2014) and Walker et al. (2020) describe how tamarisk encroachment narrowed the Yampa and Green Rivers (Colorado and Utah, USA), respectively. Friedman et al. (1996) document how Plum Creek (Colorado, USA) first widened during an extreme flood event and then narrowed as a feedback between vegetation establishment and sediment trapping rebuilt the floodplain.

These findings indicate that at least some of our scalar parameters should be better represented as functions of ecosystem dynamics. If the underlying form of our equations is correct—that is, widening through erosion and narrowing through deposition driven by lateral sediment diffusion—equations representing such ecosystem dynamics and their geomechanical consequences should be drop-in replacements for the current scalar parameters. Such explicit inclusion of ecosystem dynamics in a model currently focused around processes of fluid flow and sediment transport may yield informative results towards predicting river-channel change into the future (e.g., Diehl et al., 2020).

9.5 Implications for fluvial hazard

The model developed here describes the transient adjustment of alluvial channel width, forced by a discharge time series and constrained by bank erodibility and characteristic adjustment timescales. Although primarily formulated to capture geomorphic processes, tracking channel width has important implications for fluvial hazard and risk, particularly where infrastructure, housing, sites with potential contamination, or critical ecological assets lie close to the active channel.

https://doi.org/10.5194/egusphere-2026-1018
Preprint. Discussion started: 6 March 2026

Channel widening occurs in response to discharge events exceeding a time-varying critical value Chen and Duan (2006) and progresses at a rate controlled by both flow exceedance and an empirical bank adjustment timescale. Sequences of high flows—whether individual floods or clustered events—can therefore produce rapid width increases (Gao et al., 2021), particularly in systems with low bank cohesion (Douglas et al., 2025). These adjustments correspond to lateral migration or bank failure (Wickert et al., 2013), which may undermine infrastructure or erode adjacent land. The model identifies the timing and magnitude of such widening episodes explicitly, offering a means to anticipate periods of elevated lateral erosion hazard.

Second, channel narrowing occurs during sustained periods in which discharge remains within an intermediate range—below the threshold required to cause bank erosion but sufficiently high to enable in-channel sediment transport and deposition. These sediment-transporting but non-erosive flows result in gradual width reduction, particularly in flow regimes with limited peak discharges. The associated decline in cross-sectional area reduces conveyance capacity, raising flood stage for a given discharge and increasing the likelihood of overbank flow (Ahrendt et al., 2022). Where narrowing proceeds incrementally and unmonitored, it may lead to systematic underestimation of flood hazard (Slater et al., 2015). The model captures this behavior through a width decay term parameterized by a distinct narrowing timescale, enabling identification of discharge regimes that promote conveyance loss.

The character of flood events—particularly their duration, sequencing, and hydrograph shape—influences how channel width adjusts. Prolonged or slowly rising floods are more likely to sustain discharges above the critical erosion threshold (Darby et al., 2010), promoting progressive channel widening and increased conveyance. In contrast, short-duration or flashy floods may generate high peak discharges without sufficient time to drive significant morphological change, resulting in higher overbank hazard in previously narrowed channels. These two flood regimes—one dominated by lateral erosion and increased capacity, the other by limited erosion and frequent overbank flows—pose different challenges for infrastructure design and siting. Some assets (e.g., elevated structures or utilities on pilings) may tolerate inundation but remain highly vulnerable to lateral erosion or foundation undermining during channel migration. Conversely, others—such as infrastructure set back from the active channel—may be resistant to bank retreat but susceptible to failure during frequent overbank flooding. Designing resilient infrastructure therefore requires understanding the dominant flood regime and how it may evolve under changing discharge and geomorphic conditions (Slater et al., 2015; Ahrendt et al., 2022).

Although sediment transport is not explicitly simulated, the width adjustments described here necessarily involve sediment redistribution (Vázquez-Tarrío et al., 2024)—bank erosion during widening and sediment accretion during narrowing. These changes may alter downstream sediment budgets (Belmont et al., 2011b), reduce reservoir capacity (Streeter et al., 2024), and/or increase turbidity during high flows (Rutherfurd et al., 2020). In geomorphically active or sediment-rich catchments, such adjustments can initiate cascading hazard effects (Yanites et al., 2025): for example, width-driven erosion may trigger bank collapse, expose or undermine infrastructure, and increase sediment delivery downstream, where it can contribute to aggradation-induced flooding or reservoir sedimentation. These interactions reflect a broader class of multihazard processes in which hydrologically driven geomorphic change alters the probability or impact of subsequent events. The model developed here provides a modular and tractable framework for anticipating such transitions, linking climate and discharge variability to channel morphology and associated fluvial risk.

https://doi.org/10.5194/egusphere-2026-1018
Preprint. Discussion started: 6 March 2026

10 Conclusions

Alluvial river channels dynamically adjust their widths in response to water discharge, sediment dynamics, and local factors impacting rates of lateral erosion and deposition. Existing 0-dimensional theory describes the long-term tendency of alluvial rivers to attain an equilibrium width such that their channel-forming discharge exerts a shear stress just at the threshold of particle motion on or detachment from the banks. We expand this equilibrium theory into a 0-dimensional transient model for channel-width evolution over time, encompassing bank erosion via excess shear stress and lateral deposition via sediment diffusion towards the banks. When we drive the model with daily hydrographs from four alluvial rivers, comprising sand- and gravel-bed systems that are widening or narrowing, we reproduce observed channel-width changes.

Although simplified in both its parameterization and its treatment of the channel – as a rectangular entity with a scalar width – the channel-width formulation presented here simulates alluvial rivers' transient dynamics, thereby elucidating their forms and offering a possibility to predict their futures. Such knowledge and capacity is becoming necessary to understand the geometry and evolution of alluvial rivers. Research from the mid-twentieth century established hydraulic-geometry scaling during a time when stationary hydroclimate could be reasonably assumed, and therefore, river form largely corresponded to contemporary streamflow statistics. In the current era, both climate and land-use change are driving ongoing morphological evolution over years to decades. Alluvial river width, therefore, reflects a blend between past "remembered" streamflow and the moving target of future streamflow. By generating a method to simulate transient width change along alluvial rivers, we take a step towards a more dynamic, complete, and predictive understanding of their behavior.

Code and data availability. The source code for OTTAR is available from Wickert (2026), which is a versioned snapshot of the repository located at https://github.com/MNiMORPH/OTTAR, and may be automatically installed via pip from PyPI at https://pypi.org/project/OTTAR/. Double-Manning fitting parameters to generate rating curves are available from Wickert (2025b), which is a versioned snapshot of the repository located at https://github.com/MNiMORPH/Wickert2026-OTTAR-rating-curves. Code and required data used to generate schematic and contextual figures are available from Wickert (2025a), which is a versioned snapshot of the repository located at https://github.com/MNiMORPH/Wickert2026-OTTAR-plots. Code and data for the field examples, including that required to generate the associated figures, are available from Wickert and Jones (2026), which is an archived snapshot of the repository located at https://github.com/MNiMORPH/Wickert2026-OTTAR-data-examples.

Appendix A: Notation

A1 Coordinates

x Downstream coordinate axis: horizontal and in the direction of flow

y Cross-stream coordinate axis: horizontal and positive towards river left

u Downstream-oriented velocity

https://doi.org/10.5194/egusphere-2026-1018
Preprint. Discussion started: 6 March 2026

v Cross-stream-oriented velocity: horizontal and positive towards river left

A2 Variables

a Excess-stress exponent for erosion of cohesive material; here assumed to be 1 [–]

α Angle of water surface and river bed w.r.t. horizontal [degrees or radians]

b Channel width [m]

b_0 Initial channel width at time $t = t_0$ [m]

b_i Channel width at time $t = t_i$ [m]

$\dot{b}$ Time rate of change of channel width [m s^{-1}]

$\dot{b}_{\mathtt{w}}$ Channel widening rate: component of total width change rate [m s^{-1}]

$\dot{b}_{\mathtt{n}}$ Channel narrowing rate: component of total width change rate [m s^{-1}]

$c_{s,s}$ Concentration of suspended sediment [–]

$c_{s,b}$ Concentration of bed-load sediment in motion along the bed [–]

D Noncohesive sediment grain size [m]

D_{50} Noncohesive sediment median grain size, here used specifically for sandy bed material [m]

Δt_m Settling time for a particle, equivalent to their time spent in transit [s]

$\dot{\delta}_y$ Lateral deposition rate on a single river bank [m s^{-1}]

$\dot{\delta}_{s,y}$ Lateral deposition rate of suspended sediment on a single river bank [m s^{-1}]

$\dot{\delta}_{b,y}$ Lateral deposition rate of bed-load sediment a single river bank [m s^{-1}]

ϵ Excess bed shear stress as a multiple of bank shear stress (≈ 0.2) [–]

$\dot{\varepsilon}_y$ Lateral erosion rate of a single river bank [m s^{-1}]

$\dot{\varepsilon}_{y,c}$ Lateral erosion rate of cohesive material along a single river bank [m s^{-1}]

$\hat{\dot{\varepsilon}}_{y,c}$ Lateral erosion rate of cohesive material along a single river bank having a unit bank height (h_β) that equals the flow depth (h) [m s^{-1}]

$\dot{\varepsilon}_{y,n}$ Lateral erosion rate of noncohesive material along a single river bank [m s^{-1}]

https://doi.org/10.5194/egusphere-2026-1018
Preprint. Discussion started: 6 March 2026

f_ς "Stickiness" parameter: efficiency of suspended-load attachment and holding to the bank [–]

g Gravitational acceleration (=9.807) [m s^{-2}]

h Flow depth [m]

h_β Channel bank height [m]

k_d Rate coefficient for erosion by detachment of cohesive material; units given for stress-exponent $a = 1$ [m s^2 kg^{-1}]

k_E Efficiency coefficient for lateral erosion of noncohesive sediment [–]

k_n Efficiency coefficient for lateral deposition of noncohesive sediment [–]

k_{fp} Floodplain shape and inverse roughness coefficient [$m^{3-P_{\mathrm{fp}}}$ s^{-1}]

$K_{E,y}$ Eddy diffusivity in the y direction [m^2 s^{-1}]

λ_p Porosity (≈ 0.65) [–]

n_{ch} Manning's roughness coefficient within the channel [s $m^{-1/3}$]

P_{fp} Power-law exponent for overbank flow depth–discharge relationship [–]

$\hat{q}_{s,s,y}$ Lateral suspended-sediment flux [m s^{-1}]

q_{s,b,y^+} Unidirectional lateral bedload-transport rate towards the bank per unit downstream distance [m^2 s^{-1}]

q_{s,b,y^-} Unidirectional lateral bedload-transport rate away from the bank per unit downstream distance [m^2 s^{-1}]

Q Water discharge [m^3 s^{-1}]

ρ Water density (=1000) [kg m^{-3}]

ρ_s Sediment density (=2650) [kg m^{-3}]

R_h Channel hydraulic radius [m]

S slope of water surface and river bed (=$\tan\alpha$) [–]

t Time [s]

t_0 Initial time, corresponding to the initial width b_0 [s]

t_i A time after the initial time at which $b = b_i$ [s]

τ Shear stress [Pa]

https://doi.org/10.5194/egusphere-2026-1018
Preprint. Discussion started: 6 March 2026

τ_b Bed shear stress [Pa]

τ_β Bank shear stress [Pa]

$\tau_{c,n}$ Critical shear stress to entrain noncohesive materials [Pa]

$\tau_{c,c}$ Critical shear stress to detach and entrain cohesive materials [Pa]

τ^* Shields stress [–]

τ^*_β Bank Shields stress [–]

τ^*_b Bed Shields stress [–]

τ^*_c Critical Shields stress for noncohesive particle entrainment [–]

u_* Shear velocity [m s^{-1}]

u_{*b} Shear velocity experienced by the stream bed [m s^{-1}]

$u_{s,b}$ Downstream velocity of bed-load sediment [m s^{-1}]

$v_{s,b}$ Cross-stream velocity of bed-load sediment [m s^{-1}]

Author contributions. ADW concepualized the problem and its solutions, built the system of equations, wrote the majority of the computer code and the paper. JCJ, DL, and PHL generated field geomorphic data sets. JCJ procured hydrograph and additional river cross-sectional survey data, and provided key references and text to contextualize the study. KRB guided our use of DAKOTA for model–data fits and parameter estimation. MSVWdV aided in the conceptualization, especially with regard to river narrowing, and encouraged the development of a complete equilibrium theory. TFS helped to develop and contextualize the research. ADW, JCJ, PHL, KRB, MSVWdV, and TFS edited the manuscript.

Competing interests. The authors declare no competing financial interests.

Acknowledgements. ADW received support through a Humboldt-Forschungsstipendium from the Alexander von Humboldt-Stiftung with support from TFS. ADW, JCJ, BNİ, and PHL were supported by the US National Science Foundation (NSF) under Grant No. 1944782. JCJ received support from the University of Minnesota through the Graduate School Diversity Office, the Graduate School Fellowship Office, and the College of Science and Engineering. KRB was supported by NSF Grant No. 1725774. DL and PHL received funding support from the Minnesota Department of Natural Resources via the Lessard-Sams Outdoor Heritage Council. Idea development benefited from conversations with Jeffrey Kwang and Gary Parker. Hima Hassenruck–Gudipati and Campbell Dunn engaged with and provided useful comments on an early version of this model.

https://doi.org/10.5194/egusphere-2026-1018
Preprint. Discussion started: 6 March 2026

References

Adams, B., Bohnhoff, W., Dalbey, K., Ebeida, M., Eddy, J., Eldred, M., Hooper, R., Hough, P., Hu, K., Jakeman, J., Khalil, M., Maupin, K., Monschke, J., Ridgway, E., Rushdi, A., Seidl, D., Stephens, J., and Winokur, J.: Dakota, A Multilevel Parallel Object-Oriented Framework for Design Optimization, Parameter Estimation, Uncertainty Quantification, and Sensitivity Analysis: Version 6.13 User's Manual, Tech. Rep. SAND2020-12495, 1817318, 698667, Sandia National Laboratories, https://doi.org/10.2172/1817318, 2020.

Ahrendt, S., Horner-Devine, A. R., Collins, B. D., Morgan, J. A., and Istanbulluoglu, E.: Channel Conveyance Variability can Influence Flood Risk as Much as Streamflow Variability in Western Washington State, Water Resources Research, 58, e2021WR031 890, https://doi.org/10.1029/2021WR031890, 2022.

Allmendinger, N. E., Pizzuto, J. E., Potter, N., Johnson, T. E., and Hession, W. C.: The influence of riparian vegetation on stream width, eastern Pennsylvania, USA, Geological Society of America Bulletin, 117, 229–243, https://doi.org/10.1130/B25447.1, iSBN: 0016-7606, 2005.

Allred, T. M. and Schmidt, J. C.: Channel narrowing by vertical accretion along the Green River near Green River, Utah, GSA Bulletin, 111, 1757–1772, https://doi.org/10.1130/0016-7606(1999)111<1757:CNBVAA>2.3.CO;2, 1999.

Andrews, E. D.: Effective and bankfull discharges of streams in the Yampa River basin, Colorado and Wyoming, Journal of Hydrology, 46, 311–330, https://doi.org/10.1016/0022-1694(80)90084-0, 1980.

Andrews, E. D.: Bank stability and channel width adjustment, East Fork River, Wyoming, Water Resources Research, 18, 1184–1192, https://doi.org/10.1029/WR018i004p01184, 1982.

Andrews, E. D.: Downstream effects of Flaming Gorge Reservoir on the Green River, Colorado and Utah, GSA Bulletin, 97, 1012–1023, https://doi.org/10.1130/0016-7606(1986)97<1012:DEOFGR>2.0.CO;2, 1986.

Barnhart, K. R., Tucker, G. E., Doty, S. G., Shobe, C. M., Glade, R. C., Rossi, M. W., and Hill, M. C.: Inverting Topography for Landscape Evolution Model Process Representation: 2. Calibration and Validation, Journal of Geophysical Research: Earth Surface, 125, e2018JF004 963, https://doi.org/10.1029/2018JF004963, 2020.

Belmont, P., Gran, K., Jennings, C. E., Wittkop, C., and Day, S. S.: Holocene landscape evolution and erosional processes in the Le Sueur River, central Minnesota, in: Archean to Anthropocene: Field Guides to the Geology of the Mid-Continent of North America, edited by Miller, J. D., Hudak, G. J., Wittkop, C., and McLaughlin, P. I., 24, pp. 439–455, Geological Society of America, https://doi.org/10.1130/2011.0024(21), series Title: Geological Society of America Field Guide, 2011a.

Belmont, P., Gran, K. B., Schottler, S. P., Wilcock, P. R., Day, S. S., Jennings, C., Lauer, J. W., Viparelli, E., Willenbring, J. K., Engstrom, D. R., and Parker, G.: Large shift in source of fine sediment in the upper Mississippi river., Environmental science & technology, 45, 8804–8810, https://doi.org/10.1021/es2019109, 2011b.

Belsky, A. J., Matzke, A., and Uselman, S.: Survey of livestock influences on stream and riparian ecosystems in the western United States, Journal of Soil and Water Conservation, 54, 1999.

Beschta, R. L. and Jackson, W. L.: The Intrusion of Fine Sediments into a Stable Gravel Bed, Journal of the Fisheries Research Board of Canada, 36, 204–210, https://doi.org/10.1139/f79-030, 1979.

Blom, A., Arkesteijn, L., Chavarrías, V., and Viparelli, E.: The equilibrium alluvial river under variable flow and its channel-forming discharge, Journal of Geophysical Research: Earth Surface, 122, 1924–1948, https://doi.org/10.1002/2017JF004213, 2017.

https://doi.org/10.5194/egusphere-2026-1018
Preprint. Discussion started: 6 March 2026

Boardman, E., Danesh-Yazdi, M., Foufoula-Georgiou, E., Dolph, C. L., and Finlay, J. C.: Fertilizer, landscape features and climate regulate phosphorus retention and river export in diverse Midwestern watersheds, Biogeochemistry, 146, 293–309, https://doi.org/10.1007/s10533-019-00623-z, 2019.

Bufe, A., Paola, C., and Burbank, D. W.: Fluvial bevelling of topography controlled by lateral channel mobility and uplift rate, Nature Geoscience, 9, 706–710, https://doi.org/10.1038/ngeo2773, 2016.

Charru, F., Mouilleron, H., and Eiff, O.: Erosion and deposition of particles on a bed sheared by a viscous flow, Journal of Fluid Mechanics, 519, 55–80, https://doi.org/10.1017/S0022112004001028, 2004.

Chen, D. and Duan, J.: Modeling width adjustment in meandering channels, Journal of Hydrology, 321, 59–76, https://doi.org/10.1016/j.jhydrol.2005.07.034, 2006.

Cluer, B. and Thorne, C.: A stream evolution model integrating habitat and ecosystem benefits, River Research and Applications, 30, 135–154, https://doi.org/10.1002/rra.2631, 2014.

Daly, E. R., Fox, G. A., Miller, R. B., and Al-Madhhachi, A.-S. T.: A Scour Depth Approach for Deriving Erodibility Parameters from Jet Erosion Tests, Transactions of the ASABE, pp. 1343–1351, https://doi.org/10.13031/trans.56.10350, 2013.

Daly, E. R., Fox, G. A., Enlow, H. K., Storm, D. E., and Hunt, S. L.: Site-scale variability of streambank fluvial erodibility parameters as measured with a jet erosion test: VARIABILITY IN ERODIBILITY WITH JET EROSION TESTS, Hydrological Processes, 29, 5451–5464, https://doi.org/10.1002/hyp.10547, 2015a.

Daly, E. R., Miller, R. B., and Fox, G. A.: Modeling streambank erosion and failure along protected and unprotected composite streambanks, Advances in Water Resources, 81, https://doi.org/10.1016/j.advwatres.2015.01.004, 2015b.

Darby, S. E., Trieu, H. Q., Carling, P. A., Sarkkula, J., Koponen, J., Kummu, M., Conlan, I., and Leyland, J.: A physically based model to predict hydraulic erosion of fine-grained riverbanks: The role of form roughness in limiting erosion, Journal of Geophysical Research: Earth Surface, 115, 2010JF001 708, https://doi.org/10.1029/2010JF001708, 2010.

Davies-Colley, R. J.: Stream channels are narrower in pasture than in forest, New Zealand Journal of Marine and Freshwater Research, 31, 599–608, https://doi.org/10.1080/00288330.1997.9516792, 1997.

Dean, D. J., Topping, D., Grams, P. E., Sabol, T., and Tusso, R. B.: Suspended-sediment, bed-sediment, and in-channel topographical data at the Green River at Mineral Bottom near Canyonlands National Park, and Colorado River at Potash, UT stream gages, https://doi.org/10.5066/P9KT3GOS, 2020a.

Dean, D. J., Topping, D. J., Grams, P. E., Walker, A. E., and Schmidt, J. C.: Does Channel Narrowing by Floodplain Growth Necessarily Indicate Sediment Surplus? Lessons From Sediment Transport Analyses in the Green and Colorado Rivers, Canyonlands, Utah, Journal of Geophysical Research: Earth Surface, 125, e2019JF005 414, https://doi.org/10.1029/2019JF005414, 2020b.

Dean, D. J., Topping, D. J., Buscombe, D. D., Groten, J. T., Ziegeweid, J., Fitzpatrick, F. A., Lund, J. W., and Coenen, E. N.: The use of continuous sediment-transport measurements to improve sand-load estimates in a large sand-bedded river: The lower Chippewa River, Wisconsin, Earth Surface Processes and Landforms, 47, 2006–2023, https://doi.org/10.1002/esp.5360, 2022.

Deltares: D-Morphology User Manual, Delft3D FM Suite, Deltares, 2025.

Deng, Z. Q., de Lima, J. L. M. P., and de Lima, M. I. P.: Predicting transverse turbulent diffusivity in alluvial rivers, in: Engenharia Civil, UM, 16, 2003.

Dennis, J. E., Gay, D. M., and Walsh, R. E.: An Adaptive Nonlinear Least-Squares Algorithm, ACM Transactions on Mathematical Software, 7, 348–368, https://doi.org/10.1145/355958.355965, 1981.

https://doi.org/10.5194/egusphere-2026-1018
Preprint. Discussion started: 6 March 2026

DeZiel, B., Genet, J., Martin, I., Walerak, M., Duffey, D., Monson, B., Christopherson, D., and Nelson, S.: Cannon River Watershed Monitoring and Assessment Report, Tech. rep., Minnesota Pollution Control Agency, Saint Paul, Minnesota, USA, 2014.

Diehl, R. M., Wilcox, A. C., and Stella, J. C.: Evaluation of the integrated riparian ecosystem response to future flow regimes on semiarid rivers in Colorado, USA, Journal of Environmental Management, 271, 111 037, https://doi.org/10.1016/j.jenvman.2020.111037, 2020.

Dietrich, W. E. and Smith, J. D.: Influence of the point bar on flow through curved channels, Water Resources Research, 19, 1173–1192, https://doi.org/10.1029/WR019i005p01173, 1983.

Dietrich, W. E. and Smith, J. D.: Bed Load Transport in a River Meander, Water Resources Research, 20, 1355–1380, https://doi.org/10.1029/WR020i010p01355, 1984.

Donovan, M., Belmont, P., Notebaert, B., Coombs, T., Larson, P., and Souffront, M.: Accounting for uncertainty in remotely-sensed measurements of river planform change, Earth-Science Reviews, 193, https://doi.org/10.1016/j.earscirev.2019.04.009, 2019.

Douglas, M. M., Miller, K. L., and Lamb, M. P.: Mud cohesion governs unvegetated meander migration rates and deposit architecture, Geological Society of America Bulletin, 137, 522–540, https://doi.org/10.1130/B37315.1, 2025.

Duan, J. G.: Analytical Approach to Calculate Rate of Bank Erosion, Journal of Hydraulic Engineering, 131, https://doi.org/10.1061/(ASCE)0733-9429(2005)131:11(980), 2005.

Dunn, I. S.: Tractive Resistance of Cohesive Channels, Journal of the Soil Mechanics and Foundations Division, 85, 1–24, https://doi.org/10.1061/JSFEAQ.0000195, 1959.

Dunne, K. B. and Jerolmack, D. J.: What sets river width?, Science Advances, 6, https://doi.org/10.1126/sciadv.abc1505, 2020.

Dunne, K. B. J. and Jerolmack, D. J.: Evidence of, and a proposed explanation for, bimodal transport states in alluvial rivers, Earth Surface Dynamics, 6, 583–594, https://doi.org/10.5194/esurf-6-583-2018, 2018.

Dunne, K. B. J., Arratia, P. E., and Jerolmack, D. J.: A New Method for In Situ Measurement of the Erosion Threshold of River Channels, Water Resources Research, 58, https://doi.org/10.1029/2022WR032407, 2022.

Dury, G. H.: Principles of underfit streams, Professional Paper 452-A, United States Geological Survey, Washington, DC, series: Professional Paper, 1964.

Eaton, B. C., Church, M., and Millar, R. G.: Rational regime model of alluvial channel morphology and response, Earth Surface Processes and Landforms, 29, https://doi.org/10.1002/esp.1062, 2004.

Eke, E., Parker, G., and Shimizu, Y.: Numerical modeling of erosional and depositional bank processes in migrating river bends with self-formed width: Morphodynamics of bar push and bank pull, Journal of Geophysical Research: Earth Surface, 119, 1455–1483, https://doi.org/10.1002/2013JF003020, 2014a.

Eke, E. C., Czapiga, M. J., Viparelli, E., Shimizu, Y., Imran, J., Sun, T., and Parker, G.: Coevolution of width and sinuosity in meandering rivers, Journal of Fluid Mechanics, 760, 127–174, https://doi.org/10.1017/jfm.2014.556, iSBN: 4951176289, 2014b.

Engelund, F. and Hansen, E.: A monograph on sediment transport in alluvial streams, Teknisk Vorlag, Copenhagen, Denmark, 1967.

Foufoula-Georgiou, E., Takbiri, Z., Czuba, J. A., and Schwenk, J.: The change of nature and the nature of change in agricultural landscapes: Hydrologic regime shifts modulate ecological transitions, Water Resources Research, 51, 6649–6671, https://doi.org/10.1002/2015WR017637, arXiv: 10.1002/2014WR016527 ISBN: 1944-7973, 2015.

Friedman, J. M., Osterkamp, W. R., and Lewis, W. M.: Channel Narrowing and Vegetation Development Following a Great Plains Flood, Ecology, 77, 2167–2181, https://doi.org/10.2307/2265710, 1996.

Gao, P., Li, Z., and Yang, H.: Variable discharges control composite bank erosion in Zoige meandering rivers, CATENA, 204, 105 384, https://doi.org/10.1016/j.catena.2021.105384, 2021.

https://doi.org/10.5194/egusphere-2026-1018
Preprint. Discussion started: 6 March 2026

Germanoski, D. and Schumm, S. A.: Changes in Braided River Morphology Resulting from Aggradation and Degradation, The Journal of Geology, 101, 451–466, https://doi.org/10.1086/648239, 1993.

Gilbert, G. K.: Hydraulic-mining débris in the Sierra Nevada, Tech. Rep. 105, U.S. Geological Survey, California Water Science Center, series: Professional Paper, 1917.

Glover, R. E. and Florey, Q. L.: Stable channel profiles, Technical Report, U.S. Bureau of Reclamation, Denver, CO, USA, 1951.

Golly, A. and Turowski, J. M.: Deriving principal channel metrics from bank and long-profile geometry with the R package cmgo, Earth Surface Dynamics, 5, 557–570, https://doi.org/10.5194/esurf-5-557-2017, 2017.

Graf, W. L.: Fluvial adjustments to the spread of tamarisk in the Colorado Plateau region, GSA Bulletin, 89, 1491–1501, https://doi.org/10.1130/0016-7606(1978)89<1491:FATTSO>2.0.CO;2, 1978.

Grams, P. E. and Schmidt, J. C.: Streamflow regulation and multi-level flood plain formation: channel narrowing on the aggrading Green River in the eastern Uinta Mountains, Colorado and Utah, Geomorphology, 44, 337–360, https://doi.org/10.1016/S0169-555X(01)00182-9, 2002.

Grams, P. E. and Schmidt, J. C.: Equilibrium or indeterminate? Where sediment budgets fail: Sediment mass balance and adjustment of channel form, Green River downstream from Flaming Gorge Dam, Utah and Colorado, Geomorphology, 71, 156–181, https://doi.org/10.1016/j.geomorph.2004.10.012, 2005.

Grams, P. E., Dean, D. J., Walker, A. E., Kasprak, A., and Schmidt, J. C.: The roles of flood magnitude and duration in controlling channel width and complexity on the Green River in Canyonlands, Utah, USA, Geomorphology, 371, 107 438, https://doi.org/10.1016/j.geomorph.2020.107438, 2020.

Gran, K. and Paola, C.: Riparian vegetation controls on braided stream dynamics, Water Resources Research, 37, 3275–3283, https://doi.org/10.1029/2000WR000203, iSBN: 0043-1397, 2001.

Gran, K. B., Belmont, P., Day, S. S., Jennings, C., Johnson, A., Perg, L., and Wilcock, P. R.: Geomorphic evolution of the Le Sueur River, Minnesota, USA, and implications for current sediment loading, in: Management and Restoration of Fluvial Systems with Broad Historical Changes and Human Impacts, edited by James, L. A., Rathburn, S. L., and Whittecar, G. R., pp. 119–130, Geological Society of America, Boulder, Colorado, USA, https://doi.org/10.1130/2008.2451(08), series Title: Special Paper Issue: 451, 2009.

Güneralp, \., Abad, J. D., Zolezzi, G., and Hooke, J.: Advances and challenges in meandering channels research, Geomorphology, 163-164, 1–9, https://doi.org/10.1016/j.geomorph.2012.04.011, 2012.

Gurnell, A.: Plants as river system engineers, Earth Surface Processes and Landforms, 39, 4–25, https://doi.org/10.1002/esp.3397, 2014.

Hassan, S. T., Lubczynski, M. W., Niswonger, R. G., and Su, Z.: Surface–groundwater interactions in hard rocks in Sardon Catchment of western Spain: An integrated modeling approach, Journal of Hydrology, 517, 390–410, https://doi.org/10.1016/j.jhydrol.2014.05.026, 2014.

Hooke, R. L.: Distribution of sediment transport and shear stress in a meander bend, Journal of Geology, 83, 543–565, https://doi.org/10.1086/628140, 1975.

Hornbach, D. J., Allen, D. C., Hove, M. C., and MacGregor, K. R.: Long-term decline of native freshwater mussel assemblages in a federally protected river, Freshwater Biology, 63, 243–263, https://doi.org/10.1111/fwb.13055, 2018.

Hornbach, D. J., Hove, M. C., MacGregor, K. R., Kozarek, J. L., Sietman, B. E., and Davis, M.: A comparison of freshwater mussel assemblages along a land-use gradient in Minnesota, Aquatic Conservation: Marine and Freshwater Ecosystems, 29, 1826–1838, https://doi.org/10.1002/aqc.3167, _eprint: https://onlinelibrary.wiley.com/doi/pdf/10.1002/aqc.3167, 2019.

https://doi.org/10.5194/egusphere-2026-1018
Preprint. Discussion started: 6 March 2026

James, L. A.: Incision and morphologic evolution of an alluvial channel recovering from hydraulic mining sediment, Geological Society of America Bulletin, 103, 723–736, https://doi.org/10.1130/0016-7606(1991)103<0723:IAMEOA>2.3.CO;2, 1991.

Jones, D. R., Schonlau, M., and Welch, W. J.: Efficient Global Optimization of Expensive Black-Box Functions, Journal of Global Optimization, 13, 455–492, https://doi.org/10.1023/A:1008306431147, 1998.

Jones, J.: Historical Channel Change Caused by a Century of Flow Alteration on Sixth Water Creek and Diamond Fork River, UT, Master's thesis, Utah State University, Logan, UT, USA, https://doi.org/https://doi.org/10.26076/8475-a88e, 2018.

Jones, J., Stout, J., Belmont, P., Blythe, T., and Wilcock, P.: Updated Sixth Water/Diamond Fork data repository, https://doi.org/10.4211/hs.f3a2cbfaa5694dadab26ea3e42a21a2f, 2021.

Jones, J. C.: Data for channel width of the Cannon River, Minnesota, 1938-2017, https://doi.org/10.5281/ZENODO.10794440, 2024.

Jones, J. C., Stout, J. B., Belmont, P., Blythe, T. L., and Wilcock, P. R.: A century of channel change caused by flow augmentation on Sixth Water Creek and Diamond Fork River, Utah, USA, Earth Surface Processes and Landforms, n/a, https://doi.org/10.1002/esp.5603, 2023.

Julian, J. P. and Torres, R.: Hydraulic erosion of cohesive riverbanks, Geomorphology, 76, 193–206, https://doi.org/10.1016/j.geomorph.2005.11.003, 2006.

Justice, C., White, S. M., McCullough, D. A., Graves, D. S., and Blanchard, M. R.: Can stream and riparian restoration offset climate change impacts to salmon populations?, Journal of Environmental Management, 188, https://doi.org/10.1016/j.jenvman.2016.12.005, 2017.

Kean, J. W., Kuhnle, R. A., Smith, J. D., Alonso, C. V., and Langendoen, E. J.: Test of a Method to Calculate Near-Bank Velocity and Boundary Shear Stress, Journal of Hydraulic Engineering-ASCE, 135, 588–601, https://doi.org/10.1061/(ASCE)HY.1943-7900.0000049, iSBN: 0733-9429, 2009.

Kelly, S., Call, B., Levine, S., Belmont, P., and Larson, P.: Minnesota River Bathymetry: 2013 - 2016, https://doi.org/10.4211/hs.6cd3728f69cb4cb39c6f11baac1734ec, 2018.

Kelly, S. A.: River Hydrology, Morphology, and Dynamics in an Intensively Managed, Transient Landscape, Ph.D., Utah State University, United States – Utah, https://www.proquest.com/docview/2210132625/abstract/C4896794F5834017PQ/1, 2019.

Kelly, S. A. and Belmont, P.: High resolution monitoring of river blufferosion reveals failure mechanisms and geomorphically effective flows, Water (Switzerland), 10, https://doi.org/10.3390/w10040394, 2018.

Kelly, S. A., Takbiri, Z., Belmont, P., and Foufoula-Georgiou, E.: Human amplified changes in precipitation-runoff patterns in large river basins of the Midwestern United States, Hydrology and Earth System Sciences, 21, 5065–5088, https://doi.org/10.5194/hess-21-5065-2017, 2017.

Khanal, A., Klavon, K. R., Fox, G. A., and Daly, E. R.: Comparison of Linear and Nonlinear Models for Cohesive Sediment Detachment: Rill Erosion, Hole Erosion Test, and Streambank Erosion Studies, Journal of Hydraulic Engineering, 142, https://doi.org/10.1061/(asce)hy.1943-7900.0001147, 2016.

Klavon, K., Fox, G., Guertault, L., Langendoen, E., Enlow, H., Miller, R., and Khanal, A.: Evaluating a process-based model for use in streambank stabilization: insights on the Bank Stability and Toe Erosion Model (BSTEM), Earth Surface Processes and Landforms, 42, https://doi.org/10.1002/esp.4073, 2017.

Knox, J. C.: Valley Alluviation in Southwestern Wisconsin, Annals of the Association of American Geographers, 62, 401–410, https://doi.org/10.1111/j.1467-8306.1972.tb00872.x, 1972.

Knox, J. C.: Responses of floods to Holocene climatic change in the upper Mississippi Valley, Quaternary Research, 23, 287–300, https://doi.org/10.1016/0033-5894(85)90036-5, 1985.

https://doi.org/10.5194/egusphere-2026-1018
Preprint. Discussion started: 6 March 2026

Knox, J. C.: Sensitivity of modern and Holocene floods to climate change, Quaternary Science Reviews, 19, 439–457, https://doi.org/10.1016/S0277-3791(99)00074-8, 2000.

Konsoer, K. M., Rhoads, B. L., Langendoen, E. J., Best, J. L., Ursic, M. E., Abad, J. D., and Garcia, M. H.: Spatial variability in bank resistance to erosion on a large meandering, mixed bedrock-alluvial river, Geomorphology, 252, 80–97, https://doi.org/10.1016/j.geomorph.2015.08.002, 2016.

L. A. Clark and T. M. Wynn: Methods for Determining Streambank Critical Shear Stress and Soil Erodibility: Implications for Erosion Rate Predictions, Transactions of the ASABE, 50, 95–106, https://doi.org/10.13031/2013.22415, 2007.

Lacey, G.: Stable channels in alluvium, Minutes of the Proceedings of the Institution of Civil Engineers, 229, 259–292, https://doi.org/10.1680/imotp.1930.15592, 1930.

Lajeunesse, E., Malverti, L., and Charru, F.: Bed load transport in turbulent flow at the grain scale: Experiments and modeling, Journal of Geophysical Research: Earth Surface, 115, https://doi.org/10.1029/2009JF001628, iSBN: 0148-0227, 2010.

Lane, E. W.: The Importance of Fluvial Morphology in Hydraulic Engineering, Proceedings of the American Society of Civil Engineers, 81, 1–17, iSBN: 0879330015, 1955.

Lauer, J. W.: NCED stream restoration toolbox-Channel planform statistics, 2006.

Lauer, J. W. and Parker, G.: Net local removal of floodplain sediment by river meander migration, Geomorphology, 96, 123–149, https://doi.org/10.1016/j.geomorph.2007.08.003, 2008.

Lauer, J. W., Echterling, C., Lenhart, C., Belmont, P., and Rausch, R.: Air-photo based change in channel width in the Minnesota River basin: Modes of adjustment and implications for sediment budget, Geomorphology, 297, 170–184, https://doi.org/10.1016/j.geomorph.2017.09.005, 2017.

Laz, O. U.: Morphological assessment of a selected reach of Jamuna river by using DELFT3D model, Master's thesis, Bangladesh University of Engineering and Technology, Dhaka, Bangladesh, 2012.

Lea, D. M. and Legleiter, C. J.: Refining measurements of lateral channel movement from image time series by quantifying spatial variations in registration error, Geomorphology, 258, 11–20, https://doi.org/10.1016/j.geomorph.2016.01.009, 2016.

Lenhart, C. F., Naber, J. R., and Nieber, J. L.: Impacts of Hydrologic Change on Sandbar Nesting Availability for Riverine Turtles in Eastern Minnesota, USA, Water, 5, 1243–1261, https://doi.org/10.3390/w5031243, number: 3, 2013a.

Lenhart, C. F., Titov, M. L., Ulrich, J. S., Nieber, J. L., and Suppes, B. J.: The Role of Hydrologic Alteration and Riparian Vegetation Dynamics in Channel Evolution along the Lower Minnesota River, Transactions of the ASABE, 56, https://doi.org/10.13031/2013.42686, 2013b.

Leopold, L. B. and Maddock, T.: The hydraulic geometry of stream channels and some physiographic implications, no. 252 in Professional Paper, United States Geological Survey, Washington, D.C., 1953.

Lesser, G., Roelvink, J., Van Kester, J., and Stelling, G.: Development and validation of a three-dimensional morphological model, Coastal Engineering, 51, 883–915, https://doi.org/10.1016/j.coastaleng.2004.07.014, 2004.

Li, Z. and Quiring, S. M.: Identifying the Dominant Drivers of Hydrological Change in the Contiguous United States, Water Resources Research, 57, e2021WR029 738, https://doi.org/10.1029/2021WR029738, _eprint: https://onlinelibrary.wiley.com/doi/pdf/10.1029/2021WR029738, 2021.

Libault, F. and Pigay, H.: Causes of 20th century channel narrowing in mountain and piedmont rivers of Southeastern France, Earth Surface Processes and Landforms, 27, 425–444, https://doi.org/10.1002/esp.328, iSBN: 01979337 (ISSN), 2002.

https://doi.org/10.5194/egusphere-2026-1018
Preprint. Discussion started: 6 March 2026

Libby, D.: Assessing historical planform channel change in an altered watershed with quantification of error and uncertainty present in a GIS/aerial photography-based analysis; case study: Minnesota River, Minnesota, USA, Ph.D. thesis, Minnesota State University, Mankato, USA, volume: M.S. Issue: May, 2018.

Libby, D. J. and Larson, P. H.: Assessing Historical Planform Channel Change Within an Altered Watershed: Minnesota River, Minnesota, USA, in: Abstracts with Programs, vol. 48, p. 281243, Geological Society of America, Denver, CO, USA, 2016.

Lin, P., Pan, M., Allen, G. H., de Frasson, R. P., Zeng, Z., Yamazaki, D., and Wood, E. F.: Global Estimates of Reach-Level Bankfull River Width Leveraging Big Data Geospatial Analysis, Geophysical Research Letters, 47, e2019GL086 405, https://doi.org/10.1029/2019GL086405, 2020.

Mackin, J. H.: Concept of the Graded River, Geological Society of America Bulletin, 59, 463–512, https://doi.org/10.1130/0016-7606(1948)59[463:COTGR]2.0.CO;2, 1948.

Malatesta, L. C., Prancevic, J. P., and Avouac, J. P.: Autogenic entrenchment patterns and terraces due to coupling with lateral erosion in incising alluvial channels, Journal of Geophysical Research: Earth Surface, 122, 335–355, https://doi.org/10.1002/2015JF003797, 2017.

Manners, R. B., Schmidt, J. C., and Scott, M. L.: Mechanisms of vegetation-induced channel narrowing of an unregulated canyon river: Results from a natural field-scale experiment, Geomorphology, 211, 100–115, https://doi.org/10.1016/j.geomorph.2013.12.033, 2014.

Manning, R.: On the flow of water in open channels and pipes, Trans. Inst. Civil Eng. Ireland, 20, 1891.

Masteller, C. C. and Finnegan, N. J.: Interplay between grain protrusion and sediment entrainment in an experimental flume, Journal of Geophysical Research: Earth Surface, 122, 274–289, https://doi.org/10.1002/2016JF003943, 2017.

Métivier, F., Lajeunesse, E., and Devauchelle, O.: Laboratory rivers: Lacey's law, threshold theory, and channel stability, Earth Surface Dynamics, 5, 187–198, https://doi.org/10.5194/esurf-5-187-2017, 2017.

Montgomery, D. R. and Gran, K. B.: Downstream variations in the width of bedrock channels, Water Resources Research, 37, 1841–1846, https://doi.org/10.1029/2000WR900393, 2001.

Moody, J. A., Dungan Smith, J., and Ragan, B. W.: Critical shear stress for erosion of cohesive soils subjected to temperatures typical of wildfires, Journal of Geophysical Research: Earth Surface, 110, 1–13, https://doi.org/10.1029/2004JF000141, iSBN: 2156-2202, 2005.

Naito, K. and Parker, G.: Can Bankfull Discharge and Bankfull Channel Characteristics of an Alluvial Meandering River be Cospecified From a Flow Duration Curve?, Journal of Geophysical Research: Earth Surface, 124, 2381–2401, https://doi.org/10.1029/2018JF004971, 2019.

Naito, K. and Parker, G.: Adjustment of self-formed bankfull channel geometry of meandering rivers: modelling study, Earth Surface Processes and Landforms, 45, 3313–3322, https://doi.org/10.1002/esp.4966, 2020.

Nicholas, A. P.: Modelling the continuum of river channel patterns, Earth Surface Processes and Landforms, 38, 1187–1196, https://doi.org/10.1002/esp.3431, 2013.

Nicholas, A. P.: Modelling river and floodplain evolution using physics-based and reduced-complexity approaches, Earth Surface Processes and Landforms, 50, e70 008, https://doi.org/10.1002/esp.70008, 2025.

OpenTopography: Mapping of Diamond Fork River, UT 2017, https://doi.org/10.5069/G94T6G9J, 2018.

Parker, G.: Self-formed straight rivers with equilibrium banks and mobile bed. Part 2. The gravel river, Journal of Fluid Mechanics, 89, 127, https://doi.org/10.1017/S0022112078002505, iSBN: 1469-7645, 1978a.

Parker, G.: Self-formed rivers with stable banks and mobile bed. Part1. The sand-silt river, Journal of Fluid Mechanics, 89, 109–125, 1978b.

Parker, G.: Surface-based bedload transport relation for gravel rivers, Journal of Hydraulic Research, 28, 417–436, https://doi.org/10.1080/00221689009499058, iSBN: 0022-1686, 1990.

https://doi.org/10.5194/egusphere-2026-1018
Preprint. Discussion started: 6 March 2026

Parker, G., Shimizu, Y., Wilkerson, G. V., Eke, E. C., Abad, J. D., Lauer, J. W., Paola, C., Dietrich, W. E., and Voller, V. R.: A new framework for modeling the migration of meandering rivers, Earth Surface Processes and Landforms, 36, 70–86, https://doi.org/10.1002/esp.2113, 2011.

Partheniades, E.: Erosion and Deposition of Cohesive Soils, Journal of the Hydraulics Division, 91, https://doi.org/10.1061/JYCEAJ.0001165, 1965.

Pathak, P., , Ajay, K., , and Ahmad, S.: Temperature and precipitation changes in the Midwestern United States: implications for water management, International Journal of Water Resources Development, 33, 1003–1019, https://doi.org/10.1080/07900627.2016.1238343, _eprint: https://doi.org/10.1080/07900627.2016.1238343, 2017.

Pfeiffer, A. M., Finnegan, N. J., and Willenbring, J. K.: Sediment supply controls equilibrium channel geometry in gravel rivers, Proceedings of the National Academy of Sciences, 114, 201612 907, https://doi.org/10.1073/pnas.1612907114, arXiv: 1408.1149 ISBN: 0711232105, 2017.

Phillips, C. B. and Jerolmack, D. J.: Self-organization of river channels as a critical filter on climate signals, Science, 352, 694–697, https://doi.org/10.1126/science.aad3348, 2016.

Phillips, C. B., Masteller, C. C., Slater, L. J., Dunne, K. B. J., Francalanci, S., Lanzoni, S., Merritts, D. J., Lajeunesse, E., and Jerolmack, D. J.: Threshold constraints on the size, shape and stability of alluvial rivers, Nature Reviews Earth & Environment, 3, 406–419, https://doi.org/10.1038/s43017-022-00282-z, 2022.

Phillips, C. B., Masteller, C. C., Blaylock, J., Van Iwaarden, F., and Johnson, J. P. L.: Variability in River Width Reveals Climatic Influence on Channel Geometry, Geophysical Research Letters, 51, e2024GL111 789, https://doi.org/10.1029/2024GL111789, 2024.

Pitlick, J., Marr, J., and Pizzuto, J.: Width adjustment in experimental gravel-bed channels in response to overbank flows, Journal of Geophysical Research: Earth Surface, 118, 553–570, https://doi.org/10.1002/jgrf.20059, 2013.

Pizzuto, J., O'Neal, M., and Stotts, S.: On the retreat of forested, cohesive riverbanks, Geomorphology, 116, 341–352, https://doi.org/10.1016/j.geomorph.2009.11.008, 2010.

Pizzuto, J. E.: Flow variability and the bankfull depth of sand-bed streams of the American midwest, Earth Surface Processes and Landforms, 11, 441–450, https://doi.org/10.1002/esp.3290110409, 1986.

Pizzuto, J. E.: Numerical simulation of gravel river widening, Water Resources Research, 26, 1971–1980, https://doi.org/10.1029/WR026i009p01971, 1990.

Pizzuto, J. E.: The morphology of graded gravel rivers: a network perspective, Geomorphology, 5, 457–474, https://doi.org/10.1016/0169-555X(92)90018-J, 1992.

Pizzuto, J. E.: Channel adjustments to changing discharges, Powder River, Montana, Geological Society of America Bulletin, 106, https://doi.org/10.1130/0016-7606(1994)106<1494:catcdp>2.3.co;2, 1994.

Pollen-Bankhead, N. and Simon, A.: Hydrologic and hydraulic effects of riparian root networks on streambank stability: Is mechanical root-reinforcement the whole story?, Geomorphology, 116, 353–362, https://doi.org/10.1016/j.geomorph.2009.11.013, 2010.

Popović, P., Devauchelle, O., Abramian, A., and Lajeunesse, E.: Sediment load determines the shape of rivers, Proceedings of the National Academy of Sciences, 118, e2111215 118, https://doi.org/10.1073/pnas.2111215118, 2021.

Quigley, M. F.: Tamarix: A Case Study of Ecological Change in the American West, Oxford University Press, Incorporated, Cary, 2013.

Rinaldi, M.: Recent channel adjustments in alluvial rivers of Tuscany, central Italy, Earth Surface Processes and Landforms, 28, 587–608, https://doi.org/10.1002/esp.464, 2003.

https://doi.org/10.5194/egusphere-2026-1018
Preprint. Discussion started: 6 March 2026

Rubin, D. M. and Topping, D. J.: Quantifying the relative importance of flow regulation and grain size regulation of suspended sediment transport α and tracking changes in grain size of bed sediment β, Water Resources Research, 37, 133–146, https://doi.org/10.1029/2000WR900250, 2001.

Ruiz-Villanueva, V., Badoux, A., Rickenmann, D., Böckli, M., Schläfli, S., Steeb, N., Stoffel, M., and Rickli, C.: Impacts of a large flood along a mountain river basin: the importance of channel widening and estimating the large wood budget in the upper Emme River (Switzerland), Earth Surface Dynamics, 6, https://doi.org/10.5194/esurf-6-1115-2018, 2018.

Rutherford, J. C.: River mixing, John Wiley & Sons, Hoboken, New Jersey, USA, 1994.

Rutherfurd, I. D., Kenyon, C., Thoms, M., Grove, J., Turnbull, J., Davies, P., and Lawrence, S.: Human impacts on suspended sediment and turbidity in the River Murray, South Eastern Australia: Multiple lines of evidence, River Research and Applications, 36, 522–541, https://doi.org/10.1002/rra.3566, 2020.

Schottler, S. P., Ulrich, J., Belmont, P., Moore, R., Lauer, J. W., Engstrom, D. R., and Almendinger, J. E.: Twentieth century agricultural drainage creates more erosive rivers, Hydrological Processes, 28, 1951–1961, https://doi.org/10.1002/hyp.9738, 2014.

Schumm, S. A. and Lichty, R. W.: Channel widening and floodplain construction along Cimarron River in southwestern Kansas, Tech. Rep. 352-D, United States Geological Survey, https://doi.org/10.3133/pp352D, issue: 352-D, 1963.

Schumm, S. A., Harvey, M. D., and Watson, C. C.: Incised Channels: Morphology, Dynamics, and Control, Water Resources Publications, 1984.

Seizilles, G., Devauchelle, O., Lajeunesse, E., and Métivier, F.: Width of laminar laboratory rivers, Physical Review E, 87, 052 204, https://doi.org/10.1103/PhysRevE.87.052204, 2013.

Sheets, B. A., Paola, C., and Kelberer, J. M.: Creation and preservation of channel-form sand bodies in an experimental alluvial system, in: Sedimentary processes, environments and basins: a tribute to Peter Friend, edited by Nichols, G. J., Williams, E., and Paola, C., pp. 555–568, Blackwell, Oxford, UK, 2007.

Shields, A.: Anwendung der Aehnlichkeitsmechanik und der Turbulenzforschung auf die Geschiebebewegung, Ph.D. thesis, Technische Hochschule Berlin, Berlin, Germany, series Title: Mitteilungen Volume: 26, 1936.

Simon, A., Curini, A., Darby, S. E., and Langendoen, E. J.: Bank and near-bank processes in an incised channel, Geomorphology, 35, https://doi.org/10.1016/S0169-555X(00)00036-2, 2000.

Simon, A., Pollen-Bankhead, N., and Thomas, R. E.: Development and Application of a Deterministic Bank Stability and Toe Erosion Model for Stream Restoration, in: Geophysical Monograph Series, edited by Simon, A., Bennett, S. J., and Castro, J. M., pp. 453–474, American Geophysical Union, Washington, D. C., https://doi.org/10.1029/2010GM001006, 2011.

Slater, L. J. and Singer, M. B.: Imprint of climate and climate change in alluvial riverbeds: Continental United States, 1950-2011, Geology, 41, 1–5, https://doi.org/10.1130/G34070.1, 2013.

Slater, L. J., Singer, M. B., and Kirchner, J. W.: Hydrologic versus geomorphic drivers of trends in flood hazard, Geophysical Research Letters, 42, 370–376, https://doi.org/10.1002/2014GL062482, 2015.

Slater, L. J., Khouakhi, A., and Wilby, R. L.: River channel conveyance capacity adjusts to modes of climate variability, Scientific Reports, 9, 1–10, https://doi.org/10.1038/s41598-019-48782-1, 2019.

Smith, D. J., Wynn-Thompson, T. M., Williams, M. A., and Seiler, J. R.: Do roots bind soil? Comparing the physical and biological role of plant roots in fluvial streambank erosion: A mini-JET study, Geomorphology, 375, 107 523, https://doi.org/10.1016/j.geomorph.2020.107523, 2021.

https://doi.org/10.5194/egusphere-2026-1018
Preprint. Discussion started: 6 March 2026

Smith, D. J., Snead, M., and Thompson, T. M.: Soil Amended With Organic Matter Increases Fluvial Erosion Resistance of Cohesive Streambank Soil, Journal of Geophysical Research: Biogeosciences, 127, https://doi.org/10.1029/2021JG006723, 2022.

Stout, J. B.: Trout Habitat in an Altered Gravel-Bed River with an Augmented Flow Regime, Master's thesis, Utah State University, Logan, UT, USA, 2019.

Streeter, M. T., Schilling, K. E., Stoeffler, T., and Anderson, E.: Sedimentology of a delta formed by agricultural river discharge into a flood-control reservoir, Iowa, River Research and Applications, 40, 1584–1594, https://doi.org/10.1002/rra.4326, 2024.

Tal, M. and Paola, C.: Dynamic single-thread channels maintained by the interaction of flow and vegetation, Geology, 35, 347–350, https://doi.org/10.1130/G23260A.1, iSBN: 0091-7613, 2007.

Tal, M. and Paola, C.: Effects of vegetation on channel morphodynamics: results and insights from laboratory experiments, Earth Surface Processes and Landforms, 35, 1014–1028, https://doi.org/10.1002/esp.1908, 2010.

Thorne, C. R. and Tovey, N. K.: Stability of composite river banks, Earth Surface Processes and Landforms, 6, 469–484, https://doi.org/10.1002/esp.3290060507, 1981.

Trampush, S. M., Huzurbazar, S., and McElroy, B.: Empirical assessment of theory for bankfull characteristics of alluvial channels, Water Resources Research, 50, 9211–9220, https://doi.org/10.1002/2014WR015597, 2014.

Turowski, J. M.: Stochastic modeling of the cover effect and bedrock erosion, Water Resources Research, 45, 1–13, https://doi.org/10.1029/2008WR007262, 2009.

Turowski, J. M., Lague, D., and Hovius, N.: Cover effect in bedrock abrasion: A new derivation and its implications for the modeling of bedrock channel morphology, Journal of Geophysical Research, 112, F04 006, https://doi.org/10.1029/2006JF000697, 2007.

U.S. Congress: Renaming of the Grand River, Colorado (H.J. Res. 460), Hearing, 66th Congress, 3rd Session, Tech. Rep. 66-3, U.S. Government Printing Office, Washington, D.C., https://archives.colostate.edu/repositories/2/archival_objects/47350, backup Publisher: U.S. House of Representatives, Committee on Interstate and Foreign Commerce, 1921.

U.S. Department of Agriculture, National Agricultural Statistics Service: 2022 Census of Agriculture: United States Summary and State Data, Tech. rep., U.S. Department of Agriculture (USDA), National Agricultural Statistics Service (NASS), Washington, DC, https://www.nass.usda.gov/AgCensus/, 2024.

Vaughan, A. A., Belmont, P., Hawkins, C. P., and Wilcock, P.: Near-Channel Versus Watershed Controls on Sediment Rating Curves, Journal of Geophysical Research: Earth Surface, 122, 1901–1923, https://doi.org/10.1002/2016JF004180, _eprint: https://onlinelibrary.wiley.com/doi/pdf/10.1002/2016JF004180, 2017.

Vázquez-Tarrío, D., Ruiz-Villanueva, V., Garrote, J., Benito, G., Calle, M., Lucía, A., and Díez-Herrero, A.: Effects of sediment transport on flood hazards: Lessons learned and remaining challenges, Geomorphology, 446, 108 976, https://doi.org/10.1016/j.geomorph.2023.108976, 2024.

Walker, A. E.: Twentieth Century Channel Change of the Green River in Canyonlands National Park, Utah, Master's thesis, Utah State University, Logan, UT, USA, 2017.

Walker, A. E., Moore, J. N., Grams, P. E., Dean, D. J., and Schmidt, J. C.: Channel narrowing by inset floodplain formation of the lower Green River in the Canyonlands region, Utah, GSA Bulletin, 132, 2333–2352, https://doi.org/10.1130/B35233.1, 2020.

Wehi, P. M., Kamelamela, K. L., Whyte, K., Watene, K., and Reo, N.: Contribution of Indigenous Peoples' understandings and relational frameworks to invasive alien species management, People and Nature, 5, 1403–1414, https://doi.org/10.1002/pan3.10508, 2023.

https://doi.org/10.5194/egusphere-2026-1018
Preprint. Discussion started: 6 March 2026

Wei, G. and Yang, J. Q.: Impacts of hydrodynamic conditions and microscale surface roughness on the critical shear stress to develop and thickness of early-stage *Pseudomonas putida* biofilms, Biotechnology and Bioengineering, 120, 1797–1808, https://doi.org/10.1002/bit.28409, 2023.

Whipple, K. X. and Tucker, G. E.: Dynamics of the stream-power river incision model: Implications for height limits of mountain ranges, landscape response timescales, and research needs, Journal of Geophysical Research: Solid Earth, 104, 17 661–17 674, https://doi.org/10.1029/1999JB900120, iSBN: 1999101029, 1999.

Wickert, A. D.: Wickert2026-OTTAR-plots, https://doi.org/10.5281/ZENODO.18735973, 2025a.

Wickert, A. D.: Wickert2026-OTTAR-rating-curves, https://doi.org/10.5281/ZENODO.18736104, 2025b.

Wickert, A. D.: OTTAR, https://doi.org/10.5281/ZENODO.18736196, 2026.

Wickert, A. D. and Jones, J. C.: Wickert2026-OTTAR-data-examples, https://doi.org/10.5281/ZENODO.18736181, 2026.

Wickert, A. D. and Schildgen, T. F.: Long-profile evolution of transport-limited gravel-bed rivers, Earth Surface Dynamics, 7, 17–43, https://doi.org/10.5194/esurf-7-17-2019, 2019.

Wickert, A. D., Martin, J. M., Tal, M., Kim, W., Sheets, B., and Paola, C.: River channel lateral mobility: metrics, time scales, and controls, Journal of Geophysical Research: Earth Surface, 118, 396–412, https://doi.org/10.1029/2012JF002386, 2013.

Wickert, A. D., Jones, J. C., and Ng, G.-H. C.: Technical Note: A double-Manning approach to compute robust rating curves and hydraulic geometries, https://doi.org/10.5194/egusphere-2025-1409, 2025.

Wilcock, P. R. and McArdell, B. W.: Surface-based fractional transport rates: Mobilization thresholds and partial transport of a sand-gravel sediment, Water Resources Research, 29, 1297–1312, https://doi.org/10.1029/92WR02748, 1993.

Wobus, C. W., Tucker, G. E., and Anderson, R. S.: Self-formed bedrock channels, Geophysical Research Letters, 33, https://doi.org/10.1029/2006GL027182, iSBN: 0094-8276, 2006.

Wolman, M. G. and Gerson, R.: Relative scales of time and effectiveness of climate in watershed geomorphology, Earth Surface Processes, 3, 189–208, https://doi.org/10.1002/esp.3290030207, 1978.

Wolman, M. G. and Miller, J. P.: Magnitude and frequency of forces in geomorphic processes, Journal of Geology, 68, 54–74, 1960.

Wong, M. and Parker, G.: Reanalysis and Correction of Bed-Load Relation of Meyer-Peter and Müller Using Their Own Database, Journal of Hydraulic Engineering, 132, 1159–1168, https://doi.org/10.1061/(ASCE)0733-9429(2006)132:11(1159), iSBN: 0733-9429, 2006.

Wood, J.: Buried in bluff country: Stream and valley sedimentation in the Whitewater River Valley, Minnesota (USA), Master's thesis, University of Minnesota, Minneapolis, MN, USA, http://conservancy.umn.edu/handle/11299/259610, 2023.

Wotzka, P. and Watkins, J.: Cannon River Watershed Restoration and Protection Strategies Report, Tech. Rep. wq-ws4-23a, Minnesota Pollution Control Agency, Saint Paul, Minnesota, USA, 2016.

Yanites, B. J.: The Dynamics of Channel Slope, Width, and Sediment in Actively Eroding Bedrock River Systems, Journal of Geophysical Research: Earth Surface, 123, https://doi.org/10.1029/2017JF004405, 2018.

Yanites, B. J. and Tucker, G. E.: Controls and limits on bedrock channel geometry, Journal of Geophysical Research, 115, F04 019, https://doi.org/10.1029/2009JF001601, 2010.

Yanites, B. J., Clark, M. K., Roering, J. J., West, A. J., Zekkos, D., Baldwin, J. W., Cerovski-Darriau, C., Gallen, S. F., Horton, D. E., Kirby, E., Leshchinsky, B. A., Mason, H. B., Moon, S., Barnhart, K. R., Booth, A., Czuba, J. A., McCoy, S., McGuire, L., Pfeiffer, A., and Pierce, J.: Cascading land surface hazards as a nexus in the Earth system, Science, 388, eadp9559, https://doi.org/10.1126/science.adp9559, 2025.

Zhao, K., Coco, G., Gong, Z., Darby, S. E., Lanzoni, S., Xu, F., Zhang, K., and Townend, I.: A Review on Bank Retreat: Mechanisms, Observations, and Modeling, Reviews of Geophysics, 60, https://doi.org/10.1029/2021RG000761, 2022.

https://doi.org/10.5194/egusphere-2026-1018
Preprint. Discussion started: 6 March 2026

Table 2. Channel characteristics and parameters for the four test-case river systems. All units are SI.

Location				
River	Minnesota River	Cannon River	Green River	Diamond Fork
Gauge name	near Jordan	at Welch	[a]MB & GR	[b]Red Hollow
Gauge ID	5330000	5355200	[a]Multiple	[b]10149400
Gauge agency	USGS	USGS	USGS	USGS
Reach for width measurements	Henderson–Belle Plaine	Welch	Fort Bottom	Above Motherlode
Channel characteristics				
[d]Bank height (h_β) [m]	5.8	2.1	2.3	0.55
Slope (S)	1.0×10^{-4}	9.0×10^{-4}	2.0×10^{-4}	4.0×10^{-3}
ε	0.2	0.2	0.2	0.2
Sediment characteristics				
Median grain size (D)	0.25×10^{-3}	[e]9.6×10^{-3}	0.3×10^{-3}	[f]45×10^{-3}, 27×10^{-3}
Sediment density (ρ_s)	2650	2650	2650	2650
Critical Shields stress (τ_c^*)	0.0495	0.0495	0.0495	0.0495
Double-Manning parameters				
[g]Reference width [m]	100	45	76	10.64
Manning's n [s m$^{-1/3}$]	0.034	0.025	0.024	[f]0.034, 0.031
k_{fp} [m$^{3-P_{\mathrm{fp}}}$ s^{-1}]	138	39.7	26.4	22.3
P_{fp}	1.62	[h]5/3	1.94	[h]5/3
[i]Bed elevation [m]	0.47	0.67	0.67	1.34
Width-evolution parameters				
Initial width (b_0)	69.23	40.72	147.69	37.12
Cohesive critical shear stress ($\tau_{c,c}$)	4.99	13.73	3.01	1.03
Cohesive detachment coefficient (k_d)	0.0101	1.00×10^{-2}	0.872	0.13
Noncohesive entrainment coefficient (K_E)	3.66×10^{-5}	1.04×10^{-3}	7.35×10^{-5}	3.40×10^{-3}
"Stickiness" factor f_{s}	10^{-10}	0.032	2.80×10^{-3}	1.42×10^{-2}
Noncohesive narrowing coefficient k_n	3.88×10^{-7}	3.22×10^{-4}	0.121	3.99×10^{-3}
Width-evolution RMSE [m]	1.87	0.52	2.44	4.01

[a]The gauge at Mineral Bottom, Utah, USA (09328920: active since 2014) was used for the double-Manning parameters. The gauge at Green River, Utah, USA (09315000: active since 1894) was used for discharge measurements. The Mineral Bottom gauge has 0.8% more streamflow and a 1.1% greater standard deviation in discharge than the Green River gauge due to additional streamflow derived from the San Rafael River. Because this difference is small, we use the unmodified Green River discharge record to drive simulations of channel evolution at Mineral Bottom.

[b]To approximate water discharge at Motherlode over the period of record, we performed a two-step operation. We first used the overlap in the gauge records above (10149400, 2001–2026) and below (10149500, 1989–2001) Red Hollow to build a continuous "Above Red Hollow" discharge time series, as $Q_{\mathrm{above}} = 1.499 Q_{\mathrm{below}}^{0.9189}$. We then followed Stout (2019) to convert this time series into a a discharge time-series that would be experienced at the Motherlode site, near our study reach.

[c]Henderson to Belle Plaine; "Reach 8" from Libby (2018).

[d]From the double-Manning fit.

[e]Inverted from the in-channel Manning's n determined by Wickert et al. (2025) and constrained by an upper bound on grain size from a tributary fan.

[f]Median grain size: 45 mm at gauging station (Red Hollow); 27 mm at modeled reach (Motherlode) (Jones et al., 2023). These are associated with Manning's n values of 0.034 and 0.031, respectively (Wickert et al., 2025)

[g]Width at the gauging station used for the double-Manning rating-curve calibration.

[h]Fixed at 5/3 for Manning's equation on a flat floodplain surface because not enough data were available or used to constrain the curvature of the overbank portion of the